



Coverage Path Planning with Unmanned Aerial Vehicles over Photovoltaic Plants using Image Analysis

Andrés Fernando Pérez González
✉ afernando.perez@udea.edu.co

Thesis submitted to the Universidad de Antioquia in compliance with one of the requirements to obtain
the degree of:
Magister en Ingeniería

Director: PhD. Álvaro Jaramillo Duque, PhD. Juan Bernardo Cano

Universidad de Antioquia
Facultad de Ingenierías
Maestría en Ingeniería
Medellín
2022

Citar/How to cite

[1]

Referencia Bibtex

```
@masterthesis{Pérez2022,  
author = {Andres Pérez },  
title = {Coverage Path Planning with Unmanned Aerial Vehicles  
over Photovoltaic Plants using Image Analysis},  
school = {Universidad de Antioquia},  
type = {Tesis de maestría},  
year = {2022}  
}
```

Referencia

IEEE (2020)

Andres Pérez , "Coverage Path Planning with Unmanned Aerial Vehicles over Photovoltaic Plants using Image Analysis", Tesis de maestría, Maestría en Ingeniería, Universidad de Antioquia, Facultad de Ingenierías, 2022



Master's Degree in Engineering, Cohorte L.

Research Group (GIMEL).

Line of research: Automation and control for the rational use of energy.

Libraries Universidad de Antioquia



- Biblioteca Carlos Gaviria Díaz.
- Centro de documentación de ingeniería (CENDOI).

Universidad de Antioquia

Universidad de Antioquia - <https://www.udea.edu.co//>

Rector: John Jairo Arboleda Céspedes.

Decano/Director: Jesús Francisco Vargas Bonilla.

The content of this work corresponds to the right of expression of the authors and does not compromise the institutional thought of the University of Antioquia and does not engage its responsibility before third parties. The authors assume responsibility for copyright and related rights.

Dedications

To my family and friends for their constant support and understanding. To my advisors, for their patience.

Acknowledgements

At the end of this work that has been done over the years, I would like to say thank you to all those people who have contributed in any way to this work, supporting me to do it and inspiring me to finish it.

This work would not have been possible without the valuable help of my directors, Alvaro and Juan Bernardo. They showed patience and tenacity in guiding me through this work. Also to my reviewers for their time, complementary guidance and objectivity.

My sincere thanks to professors Orlando Carrillo and Nelson Londoño for their confidence in me.

Thanks to my teammates and friends for putting up with me in difficult moments and for the good times we have had. And, of course, to my family and my girlfriend Katherine Guerra, because they have not lost faith in me and have supported me at all times and in all circumstances.

CONTENTS

ACRONYMS AND ABBREVIATIONS	7
ABSTRACT	8
I INTRODUCTION	9
II PROBLEM STATEMENT	10
III OBJECTIVES	13
A GENERAL OBJECTIVE	13
B SPECIFIC OBJETIVES	13
IV METHODOLOGY	14
A Structure of the report	15
V Automatic Boundary Extraction for Photovoltaic Plants Using the Deep Learning U-Net Model	16
A abstract	16
B Introduction	16
C Materials and Methods	18
1 Samples Collection	18
2 Boundary Extraction Procedure	19
3 Traditional Image Processing (TIP)	19
4 Deep Learning	21
D Results and Discussion	25
1 Database Specification	25
2 Results with TIP Technique	25
3 Discussion	29
E Conclusions	29
VI Coverage path planning with semantic segmentation for UAV in PV plants	31
A abstract	31
B Introduction	31
C Materials and Methods	35
1 Deep-Learning (DL) server for segmentation	36
2 Post processing	36
3 2D coverage path planning method on The GUI interface	36
4 Simulation and Validation Platform	40
D Results and Discussion	41
1 Results with Deep server and OpenCV functions	41
2 Results of CPP Methods	42
3 Discussion	48
E Conclusions	50

VII	RESULTS AND DISCUSSION	52
A	abstract	52
B	Introduction	52
C	Summary results and scope of work	52
1	Primera Etapa	52
2	Second Stage (Objective 2 and 3)	54
VIII	GENERAL CONCLUSIONS	56
	Appendix A: Algotrithm	57
	Appendix B: Tables of Typhoon	58
	Appendix C: Tables of Iris	60
	REFERENCES	62

LIST OF TABLES

TABLE II	SUMMARY OF THE FCN AND U-NET MODEL PARAMETERS FOR THE TRAINING PROCESS	22
TABLE III	ARCHITECTURE OF THE U-NET	23
TABLE IV	COMPARISON BETWEEN THREE TECHNIQUES.	29
TABLE V	COMPARISON OF THREE CPP METHODS WITH RESPECT TO THE CPP WIDTH, SIMULATED IN A TYPHOON UAV ON THREE PV PLANTS	44
TABLE VI	COMPARISON OF THREE CPP METHODS WITH RESPECT TO THE CPP WIDTH, SIMULATED IN A 3DR IRIS UAV ON THREE PV PLANTS	48
TABLE VII	YUNEEC UAV TYPHOON TECHNICAL SPECIFICATION	58
TABLE VIII	THREE CPP METHODS USING TYPHOON UAV OVER UNIOESTE 1 PV PLANT (EXPERIMENT 1).	58
TABLE IX	THREE CPP METHODS USING TYPHOON UAV OVER ARACK PV PLANT (EXPERIMENT 2).	59
TABLE X	THREE CPP METHODS USING TYPHOON UAV OVER CSUSL PV PLANT (EXPERIMENT 3).	59
TABLE XI	3DR IRIS UAV TECHNICAL SPECIFICATION	60
TABLE XII	THREE CPP METHODS USING 3DR IRIS UAV OVER UNIOESTE 1 PV PLANT (EXPERIMENT 4).	60
TABLE XIII	THREE CPP METHODS USING 3DR IRIS UAV OVER ARACK PV PLANT (EXPERIMENT 5).	61
TABLE XIV	THREE CPP METHODS USING 3DR IRIS UAV OVER CSUSL PV PLANT (EXPERIMENT 6).	61

LIST OF FIGURES

Fig. 1	Electricity demand projection in Colombia ¹	10
Fig. 2	Problem Tree ²	14
Fig. 3	Steps of boundary extraction by image analysis with two techniques.	19
Fig. 4	FCN model.	21
Fig. 5	U-net Model.	22
Fig. 6	Steps of boundary extraction by TIP.	26
Fig. 7	Performance and metrics of the FCN model using the training and validation sets.	26
Fig. 8	Performance and metrics of the U-net model obtained using the training and validation sets.	27
Fig. 9	Evaluation with test data FCN Model.	27
Fig. 10	Evaluation with test data U-net Model.	28
Fig. 11	Stages for Coverage path planning with semantic segmentation for UAV in PV plants	35
Fig. 12	The RoI and the path generated from Initial point (I) to final point (F) by BECD	37
Fig. 13	a) Approximate cell decomposition in grids and sub grids. b), Coverage path generated with the GBSTC method.	38
Fig. 14	a) Wavefront distance transform for the selection of the initial position (I), final position (F). b) Coverage path generated using the wavefront distance transform with the selection of the initial position (I).	38
Fig. 15	UAV over the PV plant, simulated in Gazebo	40
Fig. 16	Steps of boundary extraction by DL server and OpenCV functions in Unioeste 1 PV plant.	41
Fig. 17	Steps of boundary extraction by DL server and OpenCV functions in Arak PV plant.	41
Fig. 18	Steps of boundary extraction by DL server and OpenCV functions in CSUSL PV plant.	42
Fig. 19	Performance metrics of Typhoon UAV on Unioeste PV plant (Experiment 1).	43
Fig. 20	Performance metrics of Typhoon UAV on Arak PV plant (Experiment 2).	43
Fig. 21	Performance metrics of Typhoon UAV on CSUSL PV plant (Experiment 3).	43
Fig. 22	Performance test of UAV Typhoon varying the CPP width.	45
Fig. 23	Performance metrics of 3DR Iris UAV on Unioeste PV plants (Experiment 4).	46
Fig. 24	Performance metrics of 3DR Iris UAV on Arak PV plants (Experiment 5).	46
Fig. 25	Performance metrics of 3DR Iris UAV on CSUSL PV plants (Experiment 6).	46
Fig. 26	Performance test of UAV 3DR Iris varying the CPP width.	49

ACRONYMS AND ABBREVIATIONS

Abbreviations	Term
CPP	Coverage Path Planning
UAV	Unmanned Aerial vehicle
CV	Computer Vision
PV	Photovoltaic
IoU	Interception over Union metric
DC	Dice Coefficient metric
DL	Deep Learning
BECD	Boustrophedon Exact Cellular Decomposition
GBSTC	Grid-Based Spanning Tree Coverage
GBWC	Grid-Based wavefront coverage
O&M	Operation and Maintenance
CAGR	Compound Annual Growth Rate
LCOE	The levelised cost of energy

ABSTRACT

This report proposes a strategy that determines the coverage path in unmanned air vehicles over Photovoltaic (PV) plants. The report evaluates three image analysis methods for delineating PV plants from images in a database, also assesses three coverage path planning methods, and checks the coverage path planning methods implemented in two UAVs to cover three PV plants in the Gazebo simulation environment. The manuscript consists of 8 chapters and two of these are previously published journal articles.

The first chapter evaluates some of the image analysis or computer vision methods for the delimitation of photovoltaic plants from a database, existing in the literature of the state of the art. The use of a convolutional neural network structure is proposed to perform the extraction of the PV plant (semantic segmentation) using the u-net model and then comparing the results with the models proposed by other authors. Finding that the u-net model has a more robust performance according to the most used standard metrics for the task, with respect to the other proposed methods.

The second chapter specified a method for coverage path planning in geometric areas of photovoltaic plants. Three CPP methods with several performance metrics were programmed, three simulate PV plants were modeled and two UAVs were selected. Six experiments were carried out with each PV plant varying the CPP width. From the results obtained in these experiments, one of the metrics was selected and interpolated with respect to energy consumption, a study of energy consumption was carried out for each of these possibilities, where the CPP with the lowest energy consumption is the Boustrophedon exact cell decomposition when it has the widths in a range between 0 and 7 meters, on the other hand, the Grating Based Wavefront Coverage methods has the lowest energy consumption when the CPP width is greater than 7 meters.

Concluding that UAVs with a short flight time from 10 to 15 minutes, can be used for the inspection of small PV plants (such as roofs, rooftops, canopies, and facades), where energy consumption is enough to do the inspection and return home, as well as, UAVs such as the Typhoon with up to 25 minutes of flight are appropriate for larger photovoltaic plants, also some other results were obtained from the experiments in Gazebo simulation environment.

The information generated with this work could be valuable for the inspection of photovoltaic plants, with cameras of UAV, whose resolution is less than 12 Megapixels, in addition, the results obtained served to identify a set of recommendations for future work with UAVs in Operation and maintenance (O&M) of PV plants.

Keywords: Deep Learning (DL); Unmanned Aerial Vehicle (UAV); image-processing; image segmentation; semantic segmentation; Photovoltaic (PV) plants; Coverage Path Planning (CPP)

I. INTRODUCTION

This work intends to present a novel approach for a future inspection of photovoltaic plants with unmanned aerial vehicles (UAV), since the use of these robots in this context has been in the focus of research groups. Similarly, The Research Group in Efficient Energy Management (GIMEL) does not want to be left out of this context, therefore considering the growth and the importance of photovoltaic energy, that these have been experiencing lately worldwide and regionally, it is expected that the operation and maintenance of these plants, will be a primary factor to maintain production in optimal conditions, since the number of problems related to poor production have relationship with the installation site, caused by problems such as dirt and the environment, as a consequence these tend to grow. To ensure the reliability of these plants, UAVs are used in operation and maintenance (O&M).

This work has focused on finding an automatic coverage path planning (CPP) strategy combining image analysis to perform inspection of a PV plant as used in other of robotics application fields , the result to the research question, What automatic coverage path planning strategy would be the most suitable when inspecting PV plant. Because PV plant inspections require good resolution quality when performing the task and CPPs could help to solve this problem.

As a result of experimentation with various PV plant images, CPPs and UAVs in the Gazebo simulation environment and the ROS framework, a roadmap was found that could be used to implement a CPP in a real experiment on any type of PV plant.

II. PROBLEM STATEMENT

Lately, the world has been transitioning towards renewable energy sources, due to the necessity to decrease environmental impact [1], diversify energy sources, safeguard the world energy supply. As result there has been an unprecedented growth of renewable energies in the world. In the year 2015 the market share of renewable energy was a notable 14% and it is expected a 63% market share by 2050 [2]. In 2017, one important renewable energy, the photovoltaic (PV) solar energy underwent an expansion of 98 GW while wind energy 52 GW to a global level. Solar energy has had an annual growth of 25% on a global scale. As an example of this, in 2017 there were 404 GW of installed power, however, this number increased to 505 GW in 2018 [3].

Colombia had an electricity generation capacity in the national interconnected system of 17,603.61 MW (Net effective capacity) in September 2020, according to XM [4]. 11,937.09 MW corresponds to hydroelectricity; 5,451.34 MW to thermal generation; 149.00 MW to co-generation; 18.42 MW to wind generation and 47.76 MW to solar energy. This shows the great dependence that Colombia has on hydraulic energy sources, thermal energy and the scarce investment in non-conventional sources of renewable energy [5].

The Non-Conventional Sources of Energy (FNCER standing for "Fuentes No Convencionales de Energía") in Colombia have had a 48% average growth from the year 2000 to the year 2017 [3]. Statistics from Unidad de Planeación Minero Energética de Colombia (UPME), show that during 2019 (cut to October 31st) the number of FNCER requests were 239. The number was higher that year when compared to the 215 requests in 2018 and 194 in 2017. The 239 requests received in that period show the prevalence of solar systems (219), and also the preponderance of small scale systems (less than 1MW) [6]. In short, these data show an increase in the total solar panels installed, many of them exploiting the roofs.

On the other hand, as energy projects increase so does the demand. The statistics of energy consumption in Colombia show that an average increase of 2.99% could be achieved in the period from 2016 to 2032 in the average scenario, as shown in Figure 1.

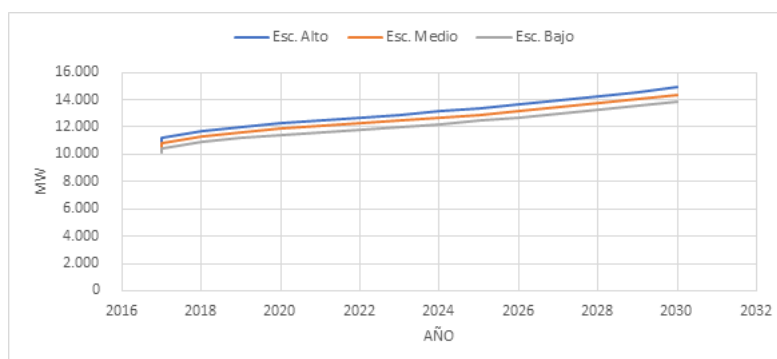


Fig. 1. Electricity demand projection in Colombia³

³Image of own creation

In order to face the growing consumer demand, it has been proposed the implementation of decentralized generation systems which facilitates the production of electricity in different areas, and which will be available to consumers [7]. In addition, the prices of PV plants have experienced a decreasing curve of 24% in the last 39 years due to the increase in their manufacturing volume. Also, the facilities produce clean net electricity for approximately 95% of their useful life, assuming that the useful life is 30 years or more [8]. Together, these systems installed in a home could, for example, provide one third of the energy needed in a day, changing from the public network to another source the power consumed by electrical appliances [9]. According to the study carried out by [10], it was concluded that the most profitable option for Colombian households is the implementation of residential PV plants without batteries or storage technologies. In this way, the user saves money while producing electric power.

PV plants can be installed on rooftops of residential or commercial buildings [11]. Likewise, they have been employed on farms to power the facilities with renewable sources [12]. These photovoltaic systems have several advantages such as the type of technology, the easiness of installation, and the time needed to recover the investment, currently ranges from 0.7 to 1.5 years [8], which makes it a profitable business.

One of the challenges that PV plants present on rooftops, and farms is access. Therefore, maintenance, and detection of possible problems in the panels such as manufacturing defects, tanning or discoloration, cracked or burned cells, corrosion, white spots, broken parts, snail traces, bubbles, joint failures, dirty spots, and other types of defects [13] are not easy to detect. Additionally, failures caused by weather, and pollution must be considered as they produce an indirect effect in increasing degradation, and decrease the energy production of the panels which affects the energy performance of the PV plant [14]. Some of these problems are addressed in this paper [15].

In order to solve these problems, research groups have been working on the development of automated systems with robots to cope with the effects caused by soiling, in fact increasing the reliability and efficiency of PV plants. Such as, in [16] was found 2,678 families of patents related to panel cleaning technologies in the period ranging from 1962 to September 2018. The vast majority, that is 65% of them, were patents on robots that work on top of the panel; 18% other type of cleaning scheme; 10% cleaning trucks; 6% autonomous cleaning robots and only 1% of these patent families included some type of aircraft that cleans the panel. Even though, checking and cleaning PV panels is a simple task that can be done manually by a technician using a cloth and a little of detergent [17]. PV installations in general are distributed over large geographic areas or are located in places difficult to access. This means that manual inspection and monitoring of the operating conditions of these PV plants can take a long time. Trained and certified personnel are needed to carry out this type of work, when it is at heights, a practice that puts the integrity of people, equipment and photovoltaic installations at risk [18].

Finally, cleaning and inspection techniques of photovoltaic systems could be combined to achieve highly complex and autonomous equipment, which not only allows the identification of faults in the panels but can also try to solve faults due to dirt, perform a cleaning of the cell, all automatically [19]. Within this group of projects, which is still under development, there are several types of designs; among these is the use of drones to perform the identification of dirt and faults as shown in [20] and then perform the

cleaning of the cells as indicated in [21]. However, within this task, there may be several challenges, one of which is that the resolution of the images and the correct flight plan are substantial to improve the quality of these images, a key factor if you do not have a high-resolution camera to find defects in photovoltaic systems [14], [22]. Consequently, an automatic coverage path planning strategy would be suitable when inspecting the PV plant, considering the width, height, and flight speed of the CPP to perform an automatic inspection of PV plants. i.e., when imaging from an UAV over PV plant [23], since most defects occur on at centimeter or millimeter scale, and this poses a challenge to currently available sensors. [24].

III. OBJECTIVES

A. GENERAL OBJECTIVE

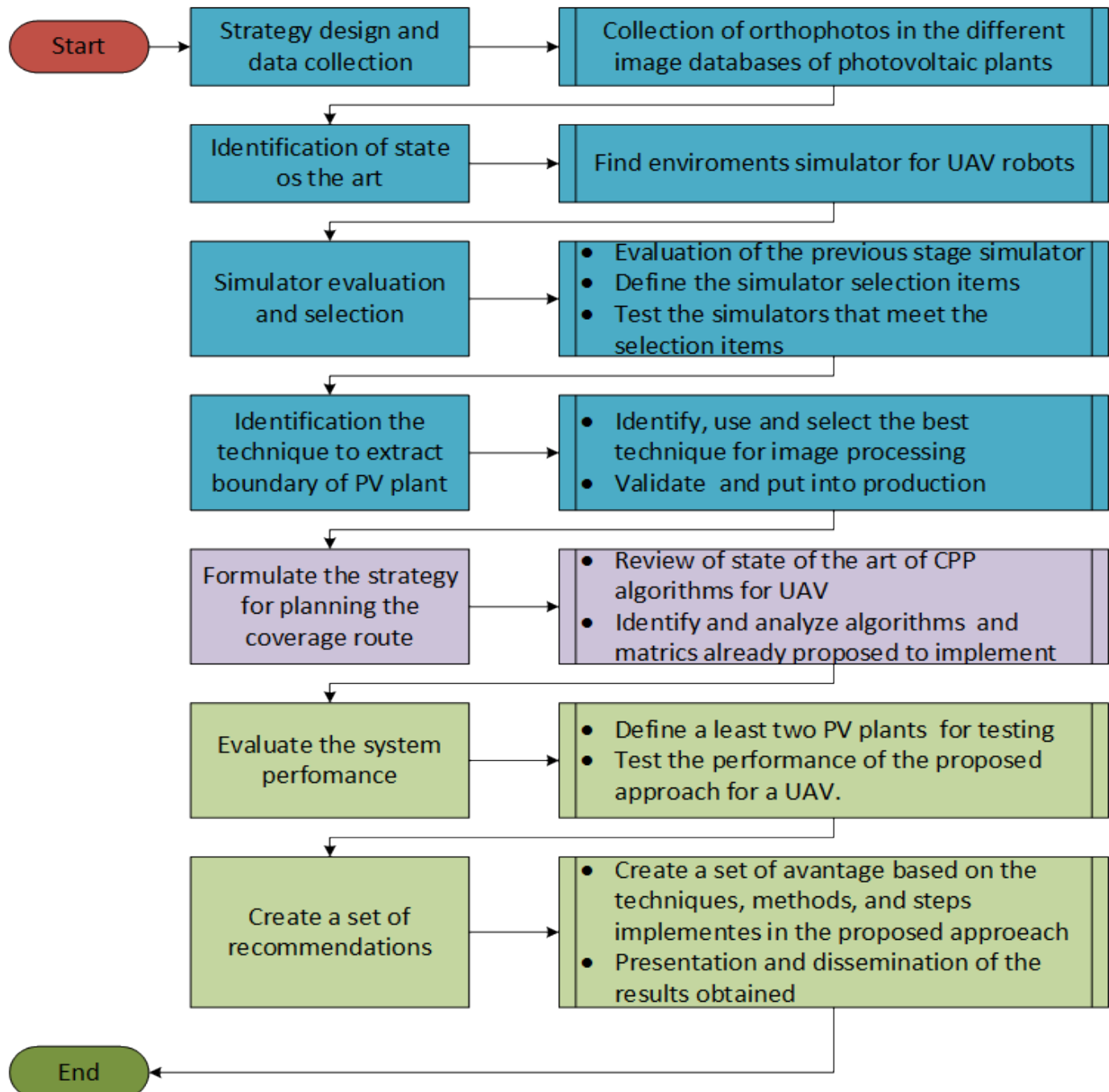
To propose a strategy that determines the coverage path for unmanned aerial vehicles, using the delimitation of photovoltaic installations through image analysis in a suitable simulation environment, for a future inspection of solar panels.

B. SPECIFIC OBJECTIVES

- To Evaluate image processing techniques for the extraction of area boundaries of photovoltaic installations.
- To specify a method for coverage routes planning over the geometric area of the PV installations.
- To evaluate the system performance in the simulation environment, verifying its operation in at least two PV installations and creating a set of recommendations to deploy the system based on a simulation environment.

IV. METHODOLOGY

For the development of this project, the methodology implemented was that of modular work, which means that first each of the parts of the system was worked on individually and finally, when each of the parts worked correctly, they were integrated to have the overall system in operation, as shown in the Figure 2, where the first specific objective of the work is shown in green, the second objective is shown in orchid and the third in olive green, each with the necessary steps for its fulfillment.

Fig. 2. Problem Tree⁴

A. Structure of the report

This work is divided into ten chapters. The first chapter was the Abstract, the second was the Introduction, the third was the problem statement, the fourth was the objectives, the fifth was the methodology used to solve the problem. The fifth chapter consists of an article already published in MDPI, where the fulfillment of objective 1 of the proposal is evidenced. The sixth chapter was also published (in the journal Applied Science of MDPI) where objectives two and three of the proposal are covered. The seventh chapter (results and discussion) is a summary of the work to clarify the reader's doubts regarding the scope and recommendations for future activities that can be carried out as a result of this project and the last chapter is the general conclusions; it presents the conclusions on the work carried out.

⁴All the following images are my own creation

V. AUTOMATIC BOUNDARY EXTRACTION FOR PHOTOVOLTAIC PLANTS USING THE DEEP LEARNING U-NET MODEL

A. abstract

Nowadays, the world is in a transition towards renewable energy solar being one of the most promising sources used today. However, Solar Photovoltaic (PV) systems present great challenges for their proper performance such as dirt and environmental conditions that may reduce the output energy of the PV plants. For this reason, inspection and periodic maintenance are essential to extend useful life. The use of unmanned aerial vehicles (UAV) for inspection and maintenance of PV plants favor a timely diagnosis. UAV path planning algorithm over a PV facility is required to better perform this task. Therefore, it is necessary to explore how to extract the boundary of PV facilities with some techniques. This research work focuses on an automatic boundary extraction method of PV plants from imagery using a deep neural network model with a U-net structure. The results obtained were evaluated by comparing them with other reported works. Additionally, to achieve the boundary extraction processes, the standard metrics Intersection over Union (IoU) and the Dice Coefficient (DC) were considered to make a better conclusion among all methods. The experimental results evaluated on the Amir dataset show that the proposed approach can significantly improve the boundary and segmentation performance in the test stage up to 90.42% and 91.42% as calculated by IoU and DC metrics, respectively. Furthermore, the training period was faster. Consequently, it is envisaged that the proposed U-Net model will be an advantage in remote sensing image segmentation.

keywords: Deep Learning (DL); Unmanned Aerial Vehicle (UAV); Photovoltaic (PV) systems; image-processing; image segmentation; semantic segmentation.

B. Introduction

In the last decade, the world began the transition towards renewable energy the harvesting of solar energy one of the most promising sources used today. Photovoltaic (PV) energy production is a fast-growing market: The Compound Annual Growth Rate (CAGR) of cumulative PV plants was 35% from year 2010 to 2019. The main reasons for this accelerated growth are: production cost of PV panels have decreased, return on investment ranging from 0.7 to 1.5 years. Some countries offer economic benefits for new facilities and the performance ratio (which informs how energy-efficient and reliable PV plants are against its theoretical production) is better nowadays. Before 2000 it was 70%, today performance ranges from 80% to 90% [1], [25].

Nonetheless, PV plants present some challenges for maintaining proper performance with failures and defects being the most common ones. In general, failures on PV systems are more concentrated in the inverters and PV modules. In the PV modules, because of dirty equipment, environmental conditions, or manufacturing problems the PV plant energy output can be reduced by 31% [13], [26], [27]. To detect

these problems, it is necessary to consider that the PV systems are commonly located on roofs, rooftops, and farms. Therefore the access, maintenance, and detection of possible problems in the panels should be carried out by trained and qualified personnel working at heights to detect these problems. These procedures can put the integrity of people, equipment, and PV Plants at risk [28]. Manual inspection can take up to 8 h/MW, depending on the number of test modules. This period can be more than double for rooftop systems, depending on the characteristics of the installation [29].

As an alternative to use trained personnel for maintenance, the use of an Unmanned Aerial Vehicle (UAV) has many advantages: it reduces the risks in maintenance labours, increases reliability, and increases effectiveness of PV plants. As a result, research teams are currently working on developing equipment that can automatically inspect and clean PV systems, as shown in [16], [30].

Compared to traditional methods, UAVs could perform an automatic inspection and monitoring with lower costs, cover larger areas, and achieve faster detection. The cameras installed on UAVs take photos [31], and through image processing, the area of the PV systems can be identified in a process called boundary extraction [32]. Once the area is identified, the ground control station calculates the Coverage Path Planning (CPP) that guides the UAV in the automatic plant inspection. Any faults are detected with the inspection, the required maintenance is scheduled.

This work focused on the boundary extraction of PV systems which is a key aspect for UAVs to conduct autonomous inspections and enhance Operation and Maintenance (O&M) [32].

Several inspections and defect detection methods have been proposed in the literature. Lately, UAVs have been used for the inspection of different PV plants, to identify the correlation between altitude and the PV panel defects detection as: shape, size, location, color, among others [14], [18], [33]–[35]. Many attempts have been committed to developing a reliable and cost-effective aerial robot with optimum efficiency over PV plant inspection [31], [36]–[38]. For autonomous inspection, large volumes of information or big data are required from PV systems. These datasets improve the inspection by means of automatic learning algorithms during the O&M process [29]. The O&M process of photovoltaic plants is an important aspect for the profitability of investors. Autonomous inspection of PV systems is a technology with great potential, mainly for large PV plants, roofs, facades and where manual techniques have notable restrictions in terms of human risk, performance, time and cost.

Traditional Image Processing (TIP) has been used extensively by other authors. In this study [14], [39]–[43], the authors used TIP to defect recognition in the inspection of photovoltaic plants. Furthermore, using HSV transformation, color filtering and segmentation, techniques have been implemented in many projects, especially for defect detection [44], to enumerate photovoltaic modules [40], [45] and identification of limits [46]. This technique has a restriction for unsupervised procedures; the user should assist in the image processing by adjusting the filter to the particular color of each target the technique aims to find. Therefore, TIP is not a proper method for autonomous aerial inspection of photovoltaic plants.

The boundary extraction is referred to as an image segmentation technique. This technique divides an image into a set of regions, and it is performed by dividing the image histogram into optimal threshold values [47], [48]. The aim is to substitute the representation of an image into something easily analyzable to obtain detailed information on the region of interest in an image and aid to annotate the scene of the object [49]. Image segmentation is necessary to identify the content of the photo. Accordingly, edge

detection is an essential tool for image segmentation [50] and can be achieved by means of traditional image processing techniques [46], [51] or through artificial vision techniques [52].

The image segmentation techniques with TIP were developed to identify objects such as the area of PV Plants out of an orthophoto [31], [53], [54]. Later, the Machine Learning (ML) and Deep Learning (DL) image segmentation techniques, also known as semantic segmentation, were proposed [55], [56]. In semantic segmentation each pixel is labeled with the class of its enclosing object or region [52]. Convolutional Neural Networks have been used for semantic segmentation, such as the Fully Convolutional Network (FCN) model [52], and U-Net network model [57], which drastically enhances the segmentation certainty compared with TIP method results, and ML technique results [55], [56].

The convolutional neural networks are used for extracting dense semantic representations from input images and to predict labels at the pixel level. To perform this task, it is necessary to obtain or create a dataset, perform a pre-processing of the data, select an appropriate model and train it based on metrics, and then evaluate the results as shown in [32]. This is a fundamental challenge in computer vision with wide applications in scene interpretation, medical imaging, robot vision, etc. [58]. Once the segmentation is done, the next step is to obtain the automatic Coverage Path Planning (CPP).

Although advances in GPS systems have improved and accuracy is around 10 cm in low-cost Real Time Kinematics (RTK) GPS systems [59]. Most of the projects use software tools that provide companies like Mission Planner [60] or development groups as QgroundControl [61]. These tools are based on simple polygonal coverage areas and a coverage pattern of zigzag path. They require time when the area is of complex geometry, or when the plant is in continuous expansion. Additionally, the programmer preloads waypoints without optimal coverage. As a consequence, to develop a real-time path-planning algorithm for an autonomous monitoring system, it is a hard task in this platform. Therefore, it is first necessary to determine the boundary of the PV plant. By taking out the boundaries of PV plants, aerial photogrammetry and mapping can be faster, effective, economical and customizable [46], they motivate to make this work. The key contributions of this work are as follows:

- In the revised literature, there is no report of U-net model to extract the boundaries of PV Plants; this work proposes such a model.
- The *IoU* and *DC* metrics were not used in previous related research works. For the trained and tested of Unet and FCN model, this work uses these metrics and finds a better solution.

This paper is structured as follows. In Section C, the necessary definitions and techniques to obtain the results are described. In Section D, the three techniques implemented for boundary extraction are compared to show the best method. Finally, in Section E some conclusions are shown.

C. Materials and Methods

1) *Samples Collection:* Before the segmentation, training samples were collected, based on the orthoimage and PV plant on-farm, rooftop, and roof photos. The samples collected to cover the spectral variability of each class of PV panel and consider the lighting variation in the scene, also in different parts of the world. For CNN, the samples were converted in a tagged image file format (.jpg) file and

mask image file format (.png) with a shape of 240×320 . The total of this dataset was found in the Amir dataset [62].

2) *Boundary Extraction Procedure:* UAVs must have a precise set of coordinates to define the coverage path planning correctly and thus fly over the total area of PV Plants in the inspection mission. To achieve this task automatically, it is necessary to explore how to extract the boundary of photovoltaic facilities with some techniques. There is a process called semantic segmentation, where each pixel is labeled with the class of its enclosing object or region, which can extract the PV Plants as a particular object in an image [32], but with the constraints that this work addresses. Two techniques have been implemented so far: Traditional Image Processing (TIP) [31] and Deep Learning (DL) [32]. Figure 3 shows the steps followed to reach that result by TIP and DL-based techniques.

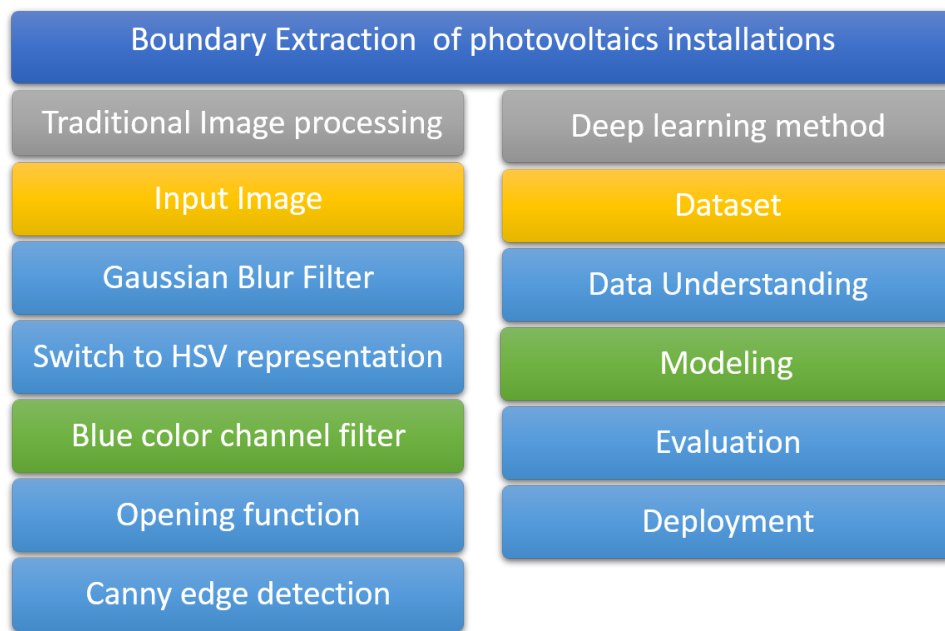


Fig. 3. Steps of boundary extraction by image analysis with two techniques.

3) *Traditional Image Processing (TIP):* The process to obtain the boundary pixels of a target can be achieved by means of traditional image processing techniques with functions that extract, increase, filter, and detect the features of an image and obtain its segmentation [46], [51]. The main stages were used to remove the borders of PV plants out of an image, as shown in Figure 3 [31]. In the first stage, the original image was filtered using “filter2D” function from OpenCV, that is a convolution filter with 5×5 averaging filter kernel, as shown at Algorithm 1. This filter is compound with various Low-Pass Filters (LPF) and High-Pass Filters (HPF). LPF helps in removing noise, blurring images. HPF filters help in finding edges in images.

In the second stage, the filtered image is transformed into the HSV (hue, saturation, and value) representation. The transformation lessens reflection caused by environmental light during aerial image collection. Furthermore, this transformation helps in the color-based segmentation required in the next stages.

In the third stage, each channel was processed separately to extract the area of the PV plants. This was achieved by applying thresholding operations on the HSV image. To extract the PV blue color out of the image, the HSV range limits for thresholding were determined: from (50, 0, 0) to (110, 255, 255). Thresholding was implemented using the `inRange` function of OpenCV.

At the fourth stage, two morphological operators were applied: the “erode” and “dilate” functions. Together these operations help to reduce noise and to better define the boundaries of the PV devices, the application of erosion followed by dilation is also known as opening operation. Erosion and dilation require a structuring element (also known as kernel) to be applied to the images. In this case, a rectangular kernel of 2×2 pixels (`MORPH_RECT,(2,2)`) was used for both operations. Lines 13, 14 and 15 from Algorithm 1 show the creation of the structuring element and the successive use of the erode and dilate functions.

Then, the “findContours” function was used to help in extracting the contours from the image. The contour can be defined as a curve joining all the continuous points in the boundary of the PV installation. The input parameters for this function are: the image (dilated image from previous stage), the type of contour to be extracted (in this case only the external contours, `RETR_EXTERNAL`) and the contour approximation method (in this case not approximation, `CHAIN_APPROX_NONE`). Finally the area was recognized using a multi-stage algorithm to detect a wide range of edges in images, known as the Canny edge detection “Canny” [63].

The pseudo-code of the Traditional Image Processing is shown in Algorithm 1, and was implemented in Python 3 using OpenCV library.

Algorithm 1: TIP algorithms.

```

1. input : A image  $Im$  of size  $w \times l$ 
2. output: A Boundary of the image
3. initialization
4. import cv 2, np
5. for  $i$  in range ( $n$ ) :
6.      $I \leftarrow cv\ 2.imread(Im)$ 
7.      $lrgb \leftarrow cv\ 2.cvtColor(I[w,l],COLOR_BRG2RGB)$ 
8.      $Kernel \leftarrow np.ones([5,5])$ 
9.      $nIldst \leftarrow cv\ 2.filter\ 2D(lrgb[w,l],-1,Kernel)$ 
10.     $lHSV \leftarrow cv\ 2.cvtColor(Ildst[w,l],COLOR_BRG2hsv) /* Transformation from$ 
11.         $RGB\ to\ HSV */$ 
12.     $LowerBlue \leftarrow np.array([55,0,0])$ 
13.     $UpperBlue \leftarrow np.array([110,255,255])$ 
14.     $mask \leftarrow cv\ 2.inRange(lHSV[w,l],LowerBlue,UpperBlue)$ 
15.     $K \leftarrow cv\ 2.getStructuringElement(MORPH_RECT,(2,2))$ 
16.     $lerosion \leftarrow cv\ 2.erode(mask[w,l],K,iteration = 3)$ 
17.     $ldilation \leftarrow cv\ 2.dilate(lerosion[w,l],K,iteration = 8)$ 
18.     $cnt \leftarrow cv$ 
19.         $2.findContours(ldilation[w,l],RETR_EXTERNAL,CHAIN_APPROX_NONE)$ 
20.     $mask2 \leftarrow cv2.zeros([w,l])$ 
21.     $cc \leftarrow cv\ 2.drawContours(mask2,cnt,-1,255,-1)$ 
22.     $edge \leftarrow cv2.Canny(cc,100,105)$ 

```

4) *Deep Learning*: Another approach to ascertain the boundaries of PV plants uses a DL-based technique which consists of several steps:

a) *Data Specifications*

The first step is to select the data for training the Neural Networks. The parameters to take into account are: PV Plants in orthophotos and aerial images with the respective masks for each image [32].

b) *Data Understanding*

The data preparation phase can be subdivided, into at least four steps. The first step is data selection inside the dataset. The second step involves correcting the individual data, which are assumed to be noisy, apparently incorrect, or absent. The third step involves resizing the data as needed. Finally, most of the available implementations assume that the data are given in a single table, so if the data are in several tables, they must be parsed together in a single one [64].

c) *Modeling*

In the literature, the semantic segmentation task has many existing models that can be selected for the desired task. In this work, two methods based on deep learning have been selected, taking into account the following criteria: the most competent for the type of task, the amount of data to be processed, the execution time, and the ease of implementation to predict each label for each pixel. The methods were selected according to [32], [65]–[68]. The FCN model was the first one selected, which was proposed by [52] and used by [32]. The network architecture is delineated in Figure 4. The second one is the U-Net model, first proposed by [57] and selected for this project. The network architecture is illustrated in Figure 5.

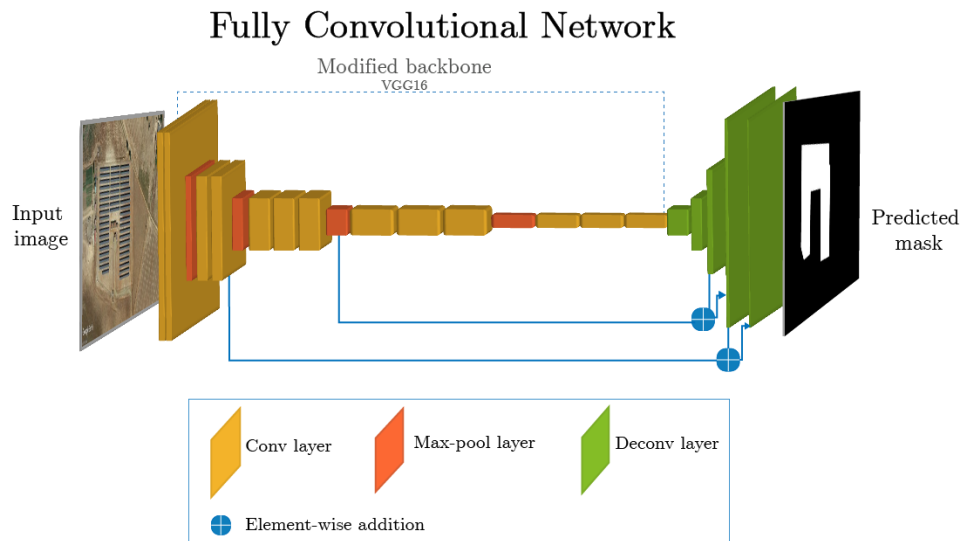


Fig. 4. FCN model.

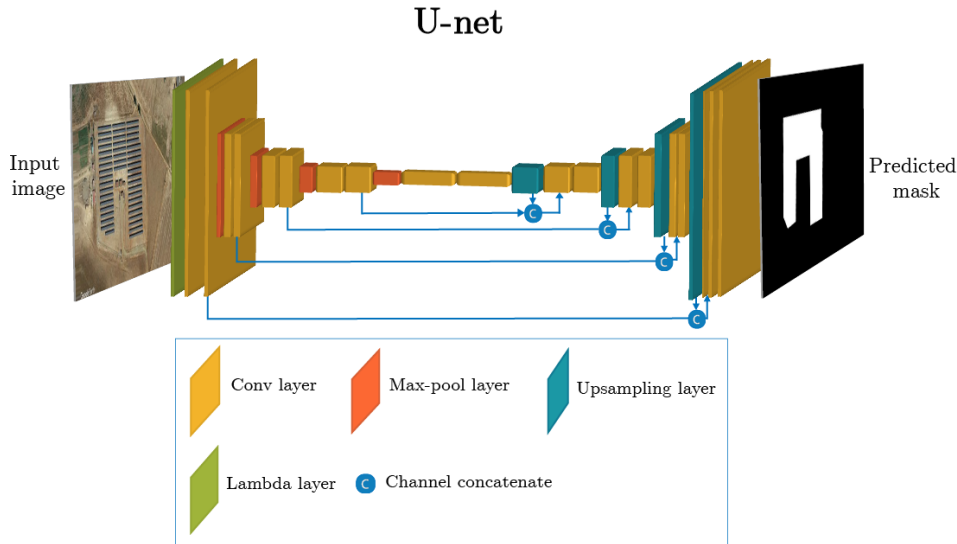


Fig. 5. U-net Model.

Fully Convolutional Network (FCN) model: This model has two blocks. The first block is a series of 13 layers in order to create a modified version of a VGG16 backbone Figure 4, which was introduced for the first time by [69]. The VGG16 backbone has 16 convolutional layers and its creators belong to the team “Visual Geometry Group”, hence its name VGG16. The backbone is the network that takes the image as input and extracts the feature map upon which the rest of the network is based. The second block consists of a series of deconvolutional layers that simply reverses the forward and backward passes of convolution. The last layer uses a softmax function to predict the probability of the category as shown in Figure 4. As a result, the input of FCN model is an RGB image, and the output is the predicted mask of the PV plants. For more details, read [52]. The parameters for the training process were depicted in Table II.

The U-net network model: This model has two blocks: a decreasing path and an increasing path, respectively, which gives it the u-shaped architecture or horizontal hourglass shape [70]. The decreasing path is a typical convolutional network that consists of repeated application of convolutions, each followed by a rectified linear unit (ReLU) and a max-pooling operation. During the decrease, the spatial information is reduced whereas feature information is increased. The increasing pathway combines the feature and spatial information through a sequence of upsampling layers followed by two layers of transposed convolution for each step [57], [71], as illustrated in Figure 5. The parameters for the training process were depicted in Table II. Its architecture is shown in Table III. The platform used for FCN and Unet models by this work was Tensorflow with Keras backend [72]. The U-net model had never been used for this kind of application so far.

TABLE II. SUMMARY OF THE FCN AND U-NET MODEL PARAMETERS FOR THE TRAINING PROCESS

Activation (last layers)	Activation (inner layers)	Optimizer	Loss funct	Metrics	Epoch	Batch size
Sigmoid	Relu	RMS	Binary_Cros	N/A	150	1
Sigmoid	Elu	Adam	Binary_Cros	IoU, Dice	15	8

The FCN and U-net models additionally have a binary cross-entropy function (H_p) to calculate the loss in the process of training the neuronal network [73]. As the problem at hand is a semantic segmentation task, Equation (1) is used. This function examines each pixel and compares the binary-predicted values vector with the binary-encoded target vector.

$$H_p(q) = -\frac{1}{N} \sum_{i=1}^N y_i \cdot \log(p(y_i)) + (1 - y_i) \cdot \log(1 - p(y_i)) \quad (1)$$

where y is the label of each pixel, it takes the value of 1 for the PV plants area and 0 to indicate other areas or elements, and $p(y)$ is the probability of the pixel belonging to the PV plants area for all N points. The Adam optimization function is used to optimize the models [74]. Because semantic segmentation is the task at hand, it is essential to implement metrics to ensure the model performs well.

H

TABLE III. ARCHITECTURE OF THE U-NET

Layer(type)	Output Shape	Parameters
Input Layer	(None, 240, 320, 3)	0
Lambda	(None, 240, 320, 3)	0
Conv2D	(None, 240, 320, 16)	448
Dropout	(None, 240, 320, 16)	0
Conv2D	(None, 240, 320, 16)	2320
MaxPooling2D	(None, 120, 160, 16)	0
Conv2D	(None, 120, 160, 32)	4640
Dropout	(None, 120, 160, 32)	0
Conv2D	(None, 120, 160, 32)	9248
MaxPooling2D	(None, 60, 80, 32)	0
Conv2D	(None, 60, 80, 64)	18496
Dropout	(None, 60, 80, 64)	0
Conv2D	(None, 60, 80, 64)	36928
MaxPooling2D	(None, 30, 40, 64)	0
Conv2D	(None, 30, 40, 128)	73856
Dropout	(None, 30, 40, 128)	0
Conv2D	(None, 30, 40, 128)	147584

Continued on next page

TABLE III – continue from previous page

Layer(type)	Output Shape	Parameters
MaxPooling2D	(None, 15, 20, 128)	0
Conv2D	(None, 15, 20, 256)	295168
Dropout	(None, 15, 20, 256)	0
Conv2D	(None, 15, 20, 256)	590080
Conv2D_Transpose	(None, 30, 40, 128)	131200
Concatenate	(None, 30, 40, 128)	73856
Conv2D	(None, 30, 40, 128)	295040
Dropout	(None, 30, 40, 128)	0
Conv2D	(None, 30, 40, 128)	147584
Conv2D_Transpose	(None, 60, 80, 64)	32832
Concatenate	(None, 60, 80, 128)	0
Conv2D	(None, 60, 80, 64)	73792
Dropout	(None, 60, 80, 64)	0
Conv2D	(None, 60, 80, 64)	36928
Conv2D_Transpose	(None, 120, 160, 32)	8224
Concatenate	(None, 120, 160, 64)	0
Conv2D	(None, 120, 160, 32)	18464
Dropout	(None, 120, 160, 32)	0
Conv2D	(None, 120, 160, 32)	9248
Conv2D_Transpose	(None, 240, 320, 16)	2064
Concatenate	(None, 240, 320, 32)	0
Conv2D	(None, 240, 320, 16)	4624
Dropout	(None, 240, 320, 16)	0
Conv2D	(None, 240, 320, 16)	2320
Conv2D	(None, 240, 320, 1)	17

d) Metrics

The metrics evaluate the similarities between the predicted mask (N) and the original mask (S). Such similarity assessment can be performed by considering spatial overlapping information, that is, by computing the true positives (TP), false positives (FP) and false negatives (FN) given by $TP = |N \cap S|$,

$FP = |N \setminus S|$, and $FN = |S \setminus N|$, respectively.

There are three standard metrics commonly employed to evaluate the effectiveness of the proposed semantic segmentation technique [48], [67], [68], [75]. The three metrics, namely, pixel accuracy (*Acc*), region Intersection over Union (*IoU*), and Dice Coefficient (*DC*).

Pixel accuracy is the ratio of correctly classified PV plants pixels to the total number of PV plants pixels in the original mask image [76], which can be mathematically represented as Equation (2).

$$Accuracy = \frac{TP}{TP + FN} \quad (2)$$

The *IoU* metric (the Jaccard index) is defined by Equation (3). This equation is a ratio between the intersection of the predicted mask N , and the original mask S and the union of both. More details can be found in [77].

$$IoU(N, S) = \frac{|N \cap S|}{|N \cup S|} = \frac{TP}{TP + FP + FN} \quad (3)$$

The *DC* metric [75], [77], [78] is expressed as Equation (4). This equation divides the intersection of the predicted mask N , and the original mask S times two by the sum of N and S .

$$DC(N, S) = \frac{2 \cdot |N \cap S|}{|N| + |S|} = \frac{2 \cdot TP}{2 \cdot TP + FP + FN} \quad (4)$$

To validate the results of the techniques described above, the FCN and U-net models were trained and their performance was evaluated by validating and testing samples of the Amir dataset [62]. The next section describes such results and compares the models in detail.

D. Results and Discussion

1) *Database Specification:* For this work, the DeepSolar [79], Google Sun-Roof [80], OpenPV [81], and Amir's databases were accessed [62]. Only the last database met the established parameters. It contained PV plants in orthophotos and aerial images with their respective masks. Furthermore, the PV plants images were from different countries around the world. Therefore, the "Amir" dataset was selected.

2) *Results with TIP Technique:* The results obtained in this work were compared with the results obtained in previous investigations where the TIP and the deep learning techniques were used alongside the FCN model [32].

The stages to obtain the results are shown in Figure 6. In the First Stage, a 2D filter was applied, depicted in Figure 6a. In the second stage, the filtered image is transformed into the HSV representation, Figure 6b. In the third stage, the blue color was filtered out, Figure 6c. At the fourth stage, the opening function

was used, as seen in Figure 6d. Finally, the area was recognized using the canny method illustrated in Figure 6e. The results were satisfactory and can be modified depending on the environment.

The results are shown in Table IV. The TIP technique was obtained by randomly selecting images out of the test dataset, then applying the functions described in the methodology section (Section C), and finally comparing the mask obtained with the original mask. The *IoU* metric obtained was 71.62% and the *DC* was 71.62%.

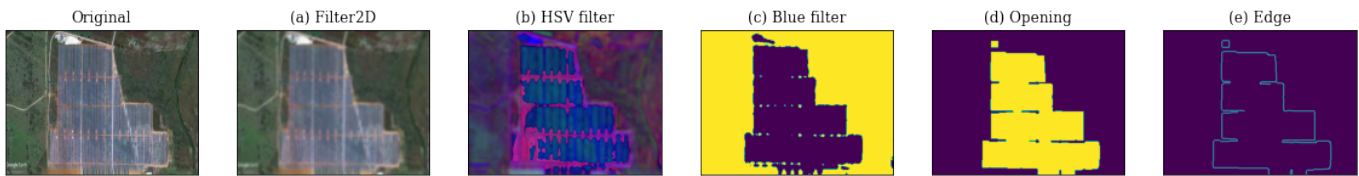


Fig. 6. Steps of boundary extraction by TIP.

c) Results with DL-Based Techniques

The training data consisted of 2864 aerial images selected at random: 90% of the training dataset in the Amir database. The validation data were the remaining 10% of the same training dataset. Figure 7a shows the loss function and *IoU* metric of the FCN model during the training and validation process. The general trend of the two curves is consistent, showing that the network converges rapidly and is stable at iteration 30, and the loss value tends to 0.04%.

Figure 7b shows the *DC* metric of the model during the training and validation stage. The general trend of the two curves is consistent at iteration 30. On the other hand, using the same metrics, the U-net model proposed in this work shows a better performance. Figure 8a shows the loss function and *IoU* metric of the model during the training and validation stage. The common trend of the two curves shows the network converges quickly and is stable at iteration 16, and the loss value tends to 0.03%.

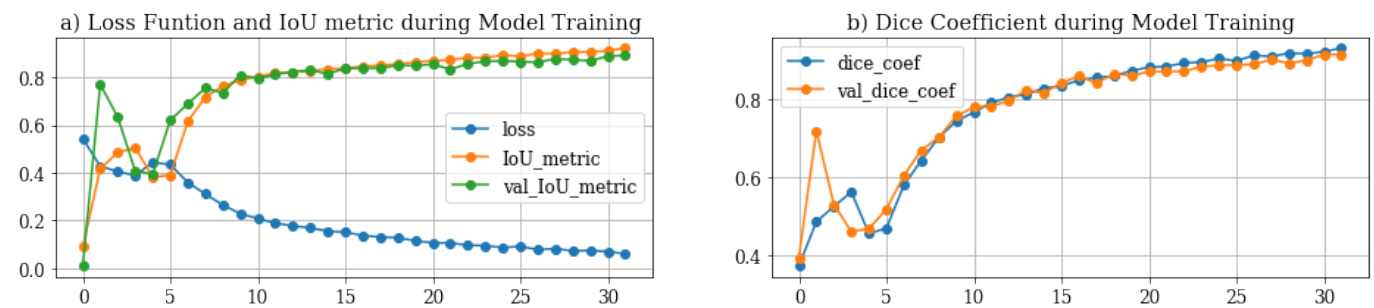


Fig. 7. Performance and metrics of the FCN model using the training and validation sets.

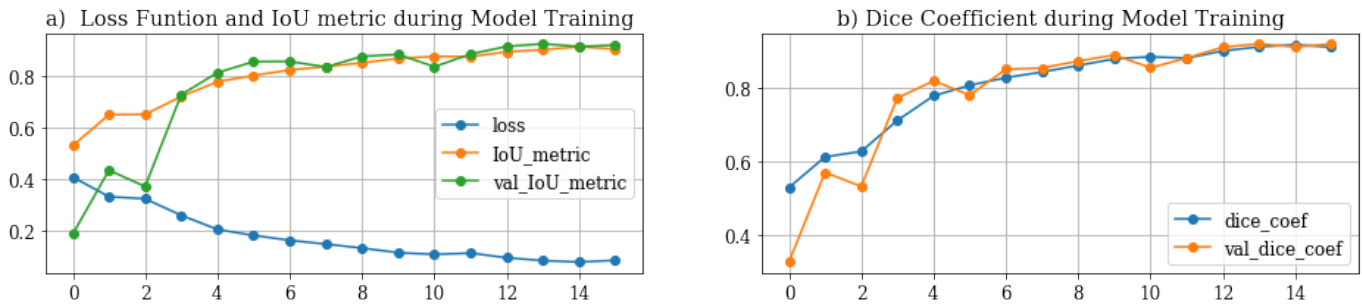


Fig. 8. Performance and metrics of the U-net model obtained using the training and validation sets.

In the evaluation stage, 716 images were used along with the trained FCN model for PV plant detection. Some relevant results are shown in Figure 9. In this figure, the columns correspond to different PV plants. The first row contains the original images; the second row, the original masks; and, the third one, the predicted masks. The images used were taken in deserted regions and vegetation zones. The FCN model detects the PV plants in vegetation zones with some false positives. As an example, the second and third predictions of Figure 9 identify a lake and vegetation as part of the PV plants. In deserted regions, PV plants are detected more precisely. Although these images have very high precision, their predicted shape does not fully correspond to the original mask. Hence, it was necessary to review the performance metrics of the algorithm [82].

The segmentation results in the evaluation stage, using the same 716 images and the trained U-Net model, are shown in Figure 10. The arrangement is the same as in the previous Figure 9. It is noteworthy that this model correctly segments the photovoltaic plant while the other model does not achieve this result, as can be seen in the second and third predictions in Figure 10.

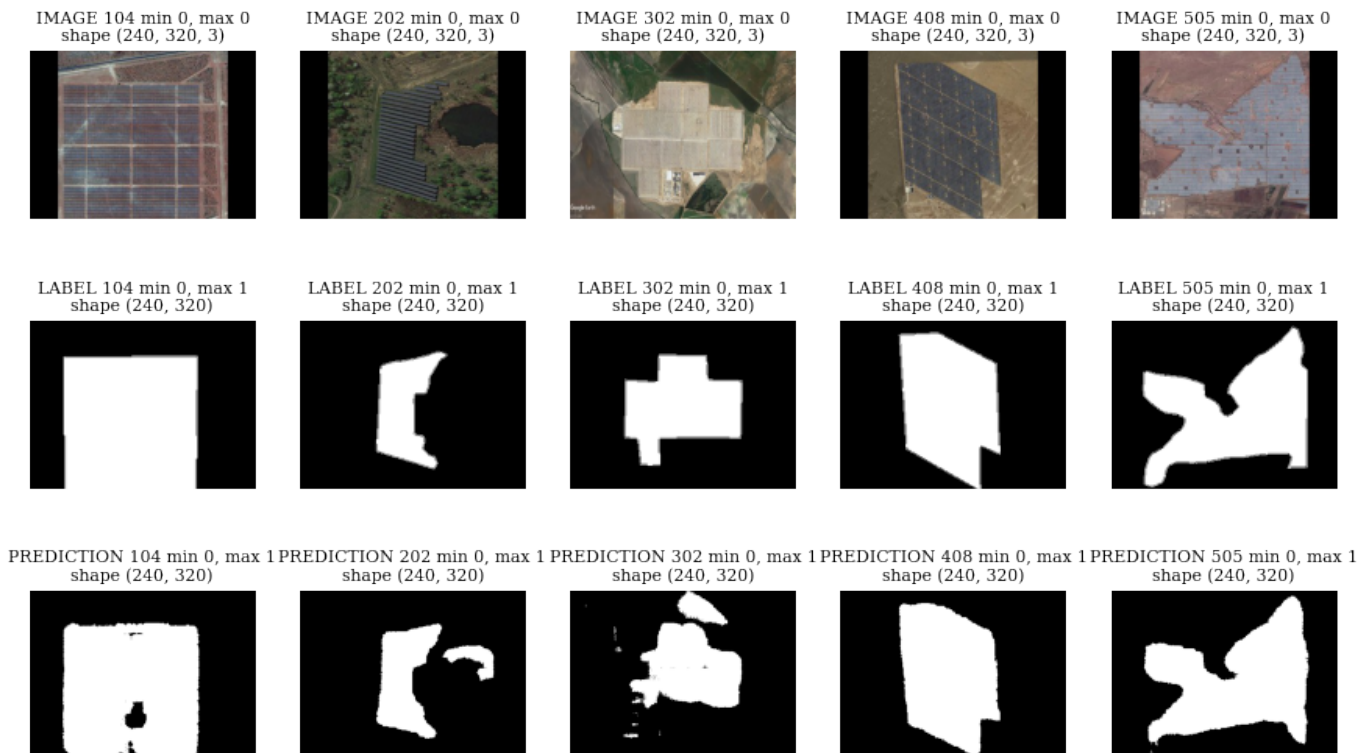


Fig. 9. Evaluation with test data FCN Model.

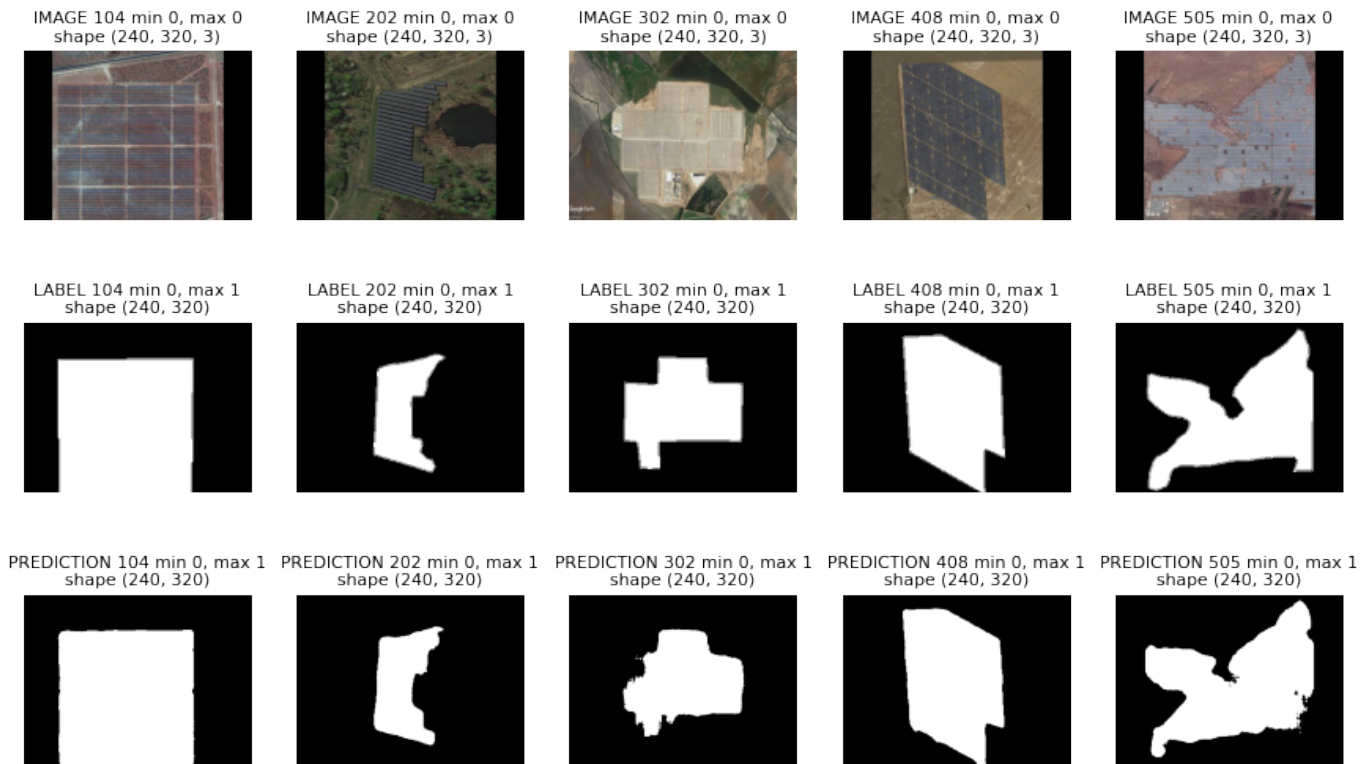


Fig. 10. Evaluation with test data U-net Model.

Afterwards, the trained model tested 716 samples. Table IV shows the results and comparison among the TIP technique, the U-net proposed model and the FCN model used by [32], which was replicated in this study. The FCN and the proposed U-net models were compared. The accuracies obtained for the FCN model in the stages of training and testing were 97.99% and 94.16% respectively [32]. For U-Net proposed, the accuracy obtained in the stages of training and testing were 97.07% and 95.44%, respectively. Both results can be seen in Table IV.

To compare the FCN model proposed by Amir [32], and the U-net model proposed in this work, the two most used metrics in semantic segmentation problems were used. The FCN model was implemented with the standard *IoU* metric, whose result for the training stage was 94.13%, and the validation stage was 90.91% and for test stage was 87.47%. The *DC* metric of the validation 92.96% and test 89.61% which deviates a little from the training 95.10%. However, using the same metrics the U-net model proposed in this work shows a better performance. The *IoU* metric obtained was 93.57% in the training stage, 93.51% in the validation stage, and 91.42% in the test stage. The *DC* metric of the validation 94.44% was almost the same as that of the training 94.03% which deviates a little from the test 91.42%. Table IV shows these results. Due to this, a difference was found between the FCN and U-net model for the first metric of 2.95% and for the second metric used of 1.81% difference was calculated. All files and logs from the experiments are available at GitHub in [83].

TABLE IV. COMPARISON BETWEEN THREE TECHNIQUES.

Parameter	TIP method	FCN used by[32]	U-Net proposed
Metrics	N/A	N/A	IoU, F1 scor
Acc train	N/A	97.99%	97.07%
Acc test	N/A	94.16%	95.44%
IoU metric	N/A	94.13%	93.57%
Dice coef metric	N/A	95.10%	94.03%
val IoU metric	N/A	90.91%	93.51%
val Dice coef	N/A	92.96%	94.44%
test IoU metric	71.62%	87.47%	90.42%
test Dice coef metric	71.62%	89.61%	91.42%

3) *Discussion:* The U-net model proposed reconstructs the segmented image and protects the original image shape characteristics by storing the grouping indices of the max-pooling layer, a process that is not done in the FCN model.

The training and testing accuracy is the percentage of pixels in the image that are classified correctly and cannot be taken as indicators of how similar the predicted PV plants and the original mask are [84]. For the purpose of comparing the similarity in the results, the *IoU* metric was used. This metric varies from 0 to 1 (0–100%) with 0 meaning no similarity and 1 meaning total similarity between original and predicted masks [82].

The U-net model proposed in this work aimed to obtain a value closer to 1 in the *IoU* metric. The iteration times show the model used is faster and therefore reliable for the training and processing stages obtaining results virtually in real time [85]. The *DC* is the other metric used in this work. This metric also ranges from 0 to 1, with 1 signifying the greatest similarity between the predicted and original masks [82]. Both metrics were used to determine if the U-net model was better than the FCN model in the validation and test stages. The values of the *IoU* and Dice metrics in Table IV showed the U-net model had a better performance when compared to the FCN model. This work was implemented with VGG16 as an encoder because it was the encoder used by Amir [32], which is a comparison work, but in future work, it is possible to use other encoders like ResNet, AlexNet, etc. [56].

Finally, the results obtained with the TIP and FCN model agree with the results obtained by other authors [14], [32]. The authors mentioned they did not use the standard metrics for these kinds of problems and the bias in the results were expected. On the contrary, this work did take these metrics into account and found satisfactory results. The U-net network increased the processing speed, veracity in the segmentation process, and the overall performance of the model.

E. Conclusions

This work used three techniques, namely, the TIP technique, the DL-based FCN and U-net models. This work applied the U-net model to PV plants. All the models were used for the extraction of the PV plants

boundaries out of an image. As a consequence, the TIP technique can be very precise but requires constant adjustment depending on the image, whereas the FCN and U-net network models are more useful when it comes to unknown PV plants.

The U-net network model is novel for this kind of problem. It allows greater processing speeds and performance when predicting the area of PV plants, also better features. The results obtained open the door for further investigation of this model in this problem.

The U-net technique turned out to be satisfactory compared to the TIP technique and the FCN model used in previous studies. The values obtained in the implemented metrics guarantee that the areas predicted for the PV plants are similar to the real ones. The results also help to predict possible false positives, such as lakes in the vicinity of photovoltaic plants. The relevant features of an object can be obtained using this technique while using the FCN technique is not possible.

VI. COVERAGE PATH PLANNING WITH SEMANTIC SEGMENTATION FOR UAV IN PV PLANTS

This third chapter was also published (in MDPI's Applied Science magazine) where objectives two and three of the proposal are covered.

A. *abstract*

Solar energy is one of the most strategic energy sources for the world's economic development. This has caused the number of solar photovoltaic plants to increase around the world; consequently, they are installed in places where their access and manual inspection are arduous and risky tasks. Recently, the inspection of photovoltaic plants has been conducted with the use of unmanned aerial vehicles (UAV). Although the inspection with UAVs can be completed with a drone operator, where the UAV flight path is purely manual or utilizes a previously generated flight path through a ground control station (GCS). However, the path generated in the GCS has many restrictions that the operator must supply. Due to these restrictions, we present a novel way to develop a flight path automatically with coverage path planning (CPP) methods. Using a DL server to segment the region of interest (RoI) within each of the predefined PV plant images, three CPP methods were also considered and their performances were assessed with metrics. The UAV energy consumption performance in each of the CPP methods was assessed using two different UAVs and standard metrics. Six experiments were performed by varying the CPP width, and the consumption metrics were recorded in each experiment. According to the results, the most effective and efficient methods are the exact cellular decomposition boustrophedon and grid-based wavefront coverage, depending on the CPP width and the area of the PV plant. Finally, a relationship was established between the size of the photovoltaic plant area and the best UAV to perform the inspection with the appropriate CPP width. This could be an important result for low-cost inspection with UAVs, without high-resolution cameras on the UAV board, and in small plants.

keywords: deep learning (DL); unmanned aerial vehicle (UAV); photovoltaic (PV) plants; semantic segmentation; coverage path planning (CPP).

B. *Introduction*

According to REN21, over the past two years, global photovoltaic (PV) plants capacities and annual additions have grown and expanded rapidly. For instance, 621 GW were installed in the year 2019 and 760 GW in the year 2020 [86], despite the reduction in electricity consumption and shifted daily demand patterns due to the COVID-19 pandemic [87]. Additionally, it has become one of the most profitable options and is an energy resource that has recently decreased in cost. As a result, solar electricity generation has grown in residential, commercial, and utility-scale projects [88]. The future of PV generation will focus on optimizing hybrid systems [89] and improving the performance of each element of the system,

as well as reducing their cost due to large-scale production [90]. Furthermore, the sector trend has been asking for low prices, and the competitive market has encouraged investment in solar PV technologies across the entire value chain, particularly in solar cells and modules, to improve efficiencies and reduce the levelized cost of energy (LCOE) [86]. As a result, PV power plants could grow almost sixfold over the next ten years, reaching a cumulative capacity of 2840 GW globally by 2030 and rising to 8519 GW by 2050, according to [91].

Thus, it is established that the number of PV plants and generated power have increased around the world. This implies specific technical challenges in their maintenance and operation (O&M) [34]. Some of these threats affect their production, which increases cost, and decreases profitability. The most common threats are the failures in the inverters and PV modules [92]. Through dirty equipment, the state of the environment, or manufacturing defects in the PV modules, PV plant energy generation can be curtailed by 31% in the worst cases [13], [26], [27].

One must consider that PV plants are commonly installed on roofs, rooftops, canopies, or facades for urban environments. Likewise, solar farms utilize rural environments, such as deserts, plains, and hills [1], [34], [93]. Depending on the location of PV plant, the manual inspection tasks could be exhausting and take up to 8 h/MW, if the number of modules are considerable. The amount of inspection time increases for solar PV plants on rooftops or canopies, by virtue to the aspects of the installation [29]. In addition, the inspection to detect threats in the panels must be conducted by trained personnel. In some cases, problems occur in elevated installations, for which special training and certificate is required. These jobs could put people and facilities at risk [28].

In recent decades, Unmanned Aerial Vehicles (UAVs) have been increasingly used in inspection and patrol tasks [16], [30], [31]. UAV-based applications for PV plants inspection have many advantages in comparison with the manual inspection methods. The main advantages are flexibility, lower cost, larger area coverage, faster detection, higher precision, and the capacity to perform a superior and automatic inspection [16], [27], [30], [94]–[96].

There are many approaches to performing an inspection with UAVs in PV modules. One of them used UAVs with a thermal imaging camera to take photos in the infrared spectrum to evaluate the UAVs parameters, such as height, speed, viewing angle, sun reflection, irradiance and temperature, all of which are necessary to perform defect inspection [97]. In a second approach, UAVs were implemented to inspect different solar PV plants, wherein analysis of the correlation between altitude and the pixel resolution was used to detect PV panel defects and features like shape, size, location, and color, among others, of a particular defect were also detected [14], [18], [33]–[35]. In a third approach, the authors proposed PV plant fault inspection with UAVs using image mosaics combined with orthophotography techniques to create a digital map; image mosaics were combined with multiple visible and/or infrared range images into a single mosaic image covering a large area [29], [44], [98]. Whereas the orthophotography technique is a vertical photograph that shows images of objects in true planimetric position [99]. Thus, these two techniques were integrated with previous works to achieve an advanced tool that allows monitoring and taking actions in the operation and maintenance (O&M) of PV plants [34]. In short, this tool has been used to detect defects and dust or dirt in PV modules [98]. Apart from this, some approaches have been developed for the detection of defects in PV modules using artificial vision techniques, machine learning,

deep learning, and the integration therewith of the previous approaches [14], [34], [45], [100]–[102]. Additionally, these approaches to planning the UAV's flight path were configured from a ground control station (GCS) program. Irrespective of these approaches, an important aspect is that the UAV should automatically follow the path to cover important points in PV plants. Many research efforts have been made to calculate the paths of and solve the waypoint planning problem for UAV inspection of solar PV plant applications [46], [103]–[105], but none of them propose the coverage path planning (CPP) as a method to complete this task. *definimos las CPP aqui vamos* The CPP, given a region of interest (RoI) in a 2D environment, consists of calculating the path that passes through each one of the points that make up the desired environment and must be found considering the limitations of movement [106], [107]. CPP is classified as a classical NP-hard problem in the field of computational complexity. These problems were initially analyzed for indoor environments with mobile robots. However, with the development of GPS, CPPs began to be used for missions with UAVs. Due to the environment in which the task is performed and the obstacles present, precise localization in the environment is an arduous task, which makes the CPP a difficult problem [108]. Additionally, it is classified as a motion planning subtopic in robotics, and has two approaches, heuristic and complete. In heuristic approaches, the robots follow a set of rules defining their behavior, but do not present a guarantee for successful full coverage. These guarantee using the cellular decomposition of the area, which involves space discretization into cells to simplify the coverage in each sub-region, unlike complete methods, which cannot afford such processing. Another important issue mentioned by the authors of reference [107] is the flight time to fully cover the area, which can be reduced using multiple robots and by reducing the number of turning maneuvers. Finally, the available RoI information is important; several approaches accept previous knowledge of the robot's respecting the search RoI (offline), while sensor-based approaches collect such information in real-time along the coverage (online) [109].

In the literature, CPP approaches are needed in several application areas, such as floor cleaning [110], agriculture [111], [112], wildfire tracking [113], bush trimming [114], power line inspection [115], photogrammetry [107], visual inspection [116], and many more. Also, many surveys regarding CPP presents several approaches and techniques to perform mostly missions with land vehicles [109], [117], [118]. The research interest in aerial robots (indoor and outdoor) has surely motivated the research of CPP [119]. This can be implemented in many UAV platforms like fixed-wing, rotary-wing, and hybrid UAV (VTOL) [107]. Rotary-wing UAVs are inexpensive and have good maneuverability, and their small payload capacity limits the weight of on-board sensors and flight time. Hence, they are more suitable for CPP missions on a small scale. Additionally, the increasing usage of UAVs in applications with complicated missions has led to CPP methods being a very active research area for single and multiple UAVs, especially recently [107], [120]–[122]. As evidenced in a previous work [111], the classic taxonomy of coverage paths in UAVs are classified into no decomposition, exact cellular decomposition, and approximate cellular decomposition. The first performs the coverage with a single UAV, for which no decomposition technique is required, because the shape of the RoI has a non-complex geometry. The second divides the free space into simple, non-overlapping regions called cells. The union of all cells fills the free space completely. The cells in which there are no obstacles are easy to cover and can be covered by the robot with simple movements. The third is based on grids. They use a representation of the environment decomposed into a collection of

uniformly squared cells [123], considering rectangular, concave, and convex polygons for RoIs. In addition to this, CPP performances were assessed with applied metrics according to [107]. The elemental approach most used to solve offline CPP problem is the area decomposition into non-overlapping sub-regions [124], to determine the appropriate visiting sequence of each sub-region and to cover each decomposed region in a back-and-forth movement to secure a complete coverage path. As a result, the methods for obtaining complete coverage of an RoI are the exact and approximate cellular decomposition methods [125]–[127]. On the other hand, image processing helps to obtain a map of the robot or RoI. Robots, such as UAVs, need to know the RoI before commencing CPP [128], which represents where the PV plants are and can be determined in a process called boundary extraction [47], [48]. Then, the deep learning (DL) image segmentation technique, also known as semantic segmentation [52], is achieved by applying deep Convolutional Neural Networks (CNN), such as U-Net network model [57], [129], which dramatically enhance the segmentation results. Once the segmentation is done and the mask is obtained or the RoI is identified, the GCS calculates the CPP that guides the UAV in the automatic plant inspection, during which it captures images of PV plants [23]. Most of the failures occur at the centimeter or millimeter level, and that poses a challenge for the inexpensive sensors available today [24]. Tests of coverage paths it can be conducted with drones in a real or simulated environment. The most viable option for this stage of the work is simulation, as verified by other research [130]–[133]. Simulation has been recognized as an important research tool; initially, simulation was an academic research tool, but with the advancement of computers, simulation has reached new levels. It is a remarkable tool that guarantees support in design, planning, analysis, and making decisions in different areas of research and development. Of course, robotics, as modern technology, has not been an exception [134], [135].

This work is focused on implementing the best strategy of coverage path planning (CPP) over PV plants with UAVs using semantic segmentation in a deep learning server to obtain the RoI. The experimental results were obtained by simulating the CPP methods and using UAVs, such as the 3DR Iris and Typhoon aerial robots.

The key contributions of this work are as follows:

- This work proposes CPPs as a novel strategy for conducting an inspection flight over a PV plant with an UAV, since there are no previous reports of such work.
- This work used three CPP methods over three PV plants, which were modeled in a simulation environment to evaluate metrics and parameters. As a result, a relationship was found between the CPP width and energy consumption, and according to that, the best CPP method to implement.
- This work proposes a hybrid CPP method that uses image processing and a DL server to find the RoI quickly and accurately, becoming a semi-automatic process.
- A free simulation tool is provided, with an interface to simulate the inspection of PV plants with UAVs.

This paper is structured as follows. In Section C, necessary definitions, and techniques to obtain the results are described. In Section D, the three CPP methods implemented are compared to show relationships among the CPP width, number of maneuvers, and energy consumption, with the aim of finding the best CPP method to implement. Finally, in Section E some conclusions are given..

C. Materials and Methods

In this work, three PV power plants were select that met the image requirements of no light distortions, non-complex geometry and grouped panels. These plants are in different parts of the world. The first PV plant has an area of 35, 975 square meter, located in Brazil (-22.119948323621525, -51.44666423682603), known as Usina Solar Unioeste 1 [136]. The second PV plant has an area of 25, 000 square meters, located in Iran (34.0504329771808, 49.796635265177294), known as Arack power plant [46] . The third PV plant is in the United States (38.55989816199527, -121.42374978032115), the plant has an area of 1, 344 square meters and is part of PV plant located on the roof of the California State University Sacramento Library (CSUSL) [137].

These plants were subjected to a series of processing stages, as shown in Figure 11. The RoIs were obtained from Google Maps satellite images with a predefined altitude, and limits, from which the image (Input Image) of the desired PV plant was obtained as the first stage, shown in the Figure 11. In the second stage, the image was entered into the DL server that was developed in this work, taking in to account the previous work [129]. The DL server was launched with TensorFlow [138] and flask [139]. This stage obtains a mask (Image Segmentation) of the PV plant, as shown in Figure 11. In the third stage was necessary to apply a series of OpenCV functions (Post-Processing), as referenced in Algorithm 2 in the appendix A, to adjust the mask (output mask) to the PV plant area, as seen in Figure 11. Then, the output mask or RoI was introduced in the GUI interface, where the CPP method was selected to internally execute. Later, the path GPS positions (CPP computed) were sent to the UAV through MAVlink commands [140], [141]. The UAV executed these commands in the Gazebo platform (CPP simulation) and, at the same time, the simulation data was fed back the GUI interface. Simultaneously all GPS points reached by the UAV were drawn in the GCS platform (CPP). In this stage, the trajectory was validated. Each stage is described in greater detail in the following sections.

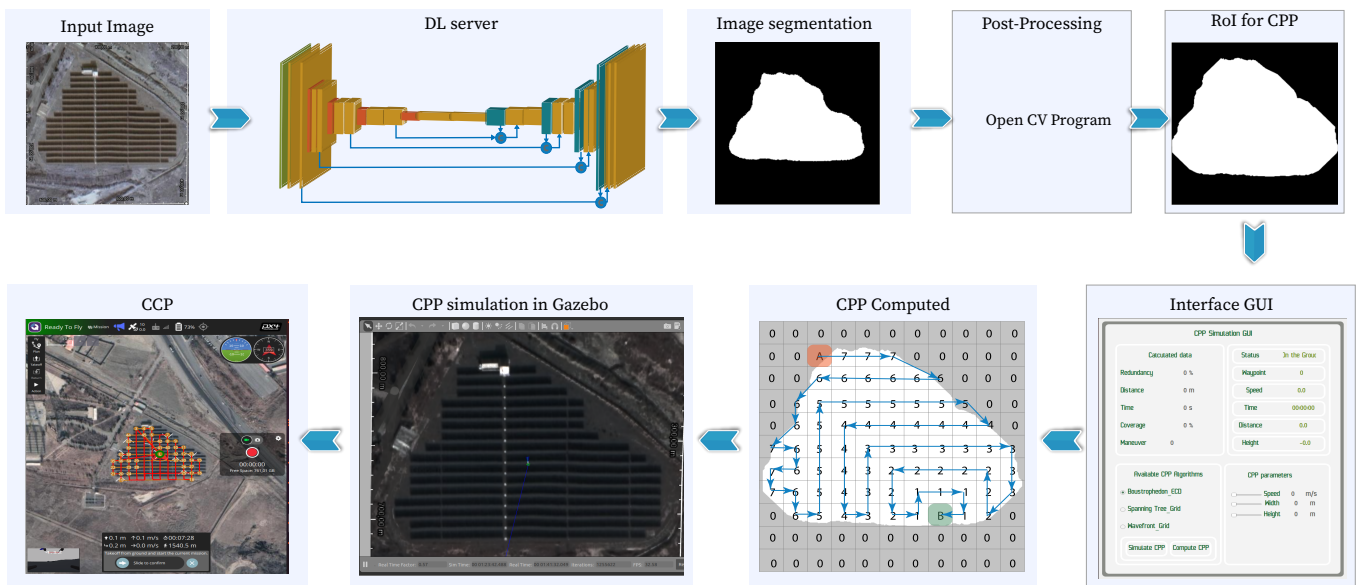


Fig. 11. Stages for Coverage path planning with semantic segmentation for UAV in PV plants .

1) *Deep-Learning (DL) server for segmentation:* The Deep-Learning (DL) server for segmentation was necessary to extract the RoIs from the Google Maps images. Additionally, the server was used to achieve this task automatically with the process called semantic segmentation, wherein each pixel is labeled with the class of its enclosing object [32], [129]. In previous work, a convolutional neural network was proposed, wherein a public database was used; this data was prepared, resized for training, and assessed with two network structures. The U-net network had the best performance, in terms of metrics, in the semantic segmentation task [129]. Then a DL server was employed to perform image segmentation and obtain the RoI [142].

2) *Post processing:* In this step, a set of OpenCV functions were applied with Python 3.7. For example, in the first function, morphological operators like “Erode” and “Dilate” were applied to the images, then the “FindContours” function was applied to help extract their contours. The contour can be defined as a curve that joins all the continuous points at the boundary of the PV installation. So, the “ContourArea” function was then used to find the area of the previous contour. Following this pattern, the area was compared with 400 others to filter the bigger area and eliminate the little areas belonging to false positives. Then the “ApproxPolyDP” function was used to approximate a shape of the contour to another shape with fewer vertices. Subsequently, the “DrawContour” function was used to draw the resulting contour [143], [144]. Finally, the “Erode” morphological operators were used again, to expand the known area and compensate for the limitations of the mask with regard to the CPP method and some faulty occurrences caused by the false positives of the DL server. The pseudocode of the openCV functions used is shown in algorithm 2 in the Appendix A.

3) *2D coverage path planning method on The GUI interface:* In previous studies of CPPs, there were many existing methods from which to select to solve the CPP problem. In this work, three methods based on CPP were selected, considering the following criteria: time of execution, ease of implementation, and more, which were used to cover the RoI. The methods were selected according to [106], [107]. The boustrophedon exact cellular decomposition (BECD), which was proposed by [145], was the first selected. The CPP method is delineated in Figure 12.

The second was grid-based spanning tree coverage (GBSTC), which works with cellular decomposition, first proposed by [146], and depicted in Figure 13.

The third method selected for this project was grid-based wavefront coverage (GBWC), first proposed by [147]. The method is illustrated in Figure 14. Each of these CPP methods is explained in more detail in the following sections.

a).The boustrophedon exact cellular decomposition (BECD) Method: This method takes the robot’s free space and obstacles and splits them into cells. These cells are covered by the robot using a back-and-forth pattern from the initial point to the final point, using maneuvers of 90 degrees to change direction from south to north or vice versa, as shown in Figure 12. This method improves the trapezoid decomposition technique, as it exploits the structure of the polygon to determine the start and end of an obstacle, and thus is able to divide the free space into a few cells that do not require a redundant step, and it permits the coverage of curved areas [145].

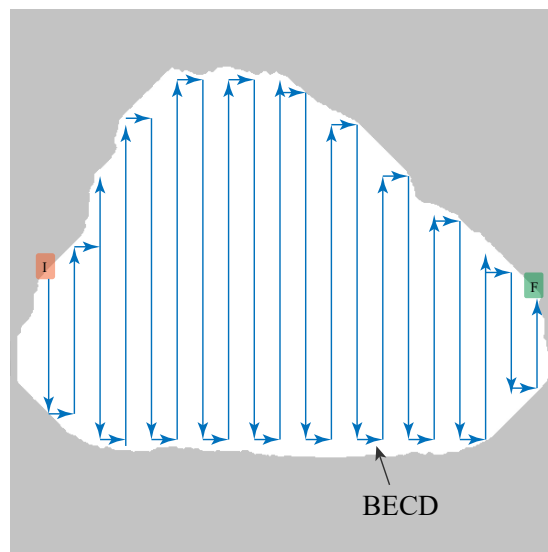


Fig. 12. The RoI and the path generated from Initial point (I) to final point (F) by BECD

b). Grid-Based Spanning Tree Coverage (GBSTC): This method is based on approximate cell decomposition and differs from the previous method in that the following postulates were considered. First, the method divides the space into grids of side L . Second, the robot only moves in perpendicular directions to the sides of the grid. Third, every grid is subdivided into four grids of side $L/2$. Finally, GBSTC discards space that is partly occupied by obstacles. Consequently, considering these previous postulates, the method consists of several stages: in the first stage, a graphic structure is defined, $S(N, E)$, where N is nodes, defined as the central point of each grid, and E is edges, defined as the line segments connecting the centers of adjoining grids, as shown in Figure 13a. In the second stage, the method builds a spanning tree for S , and employs this tree to plan a cover path as follows. Starting in grid I with a sub-grid of side $L/2$, the robot begins by travelling between adjoining sub-grids along a path that moves around the spanning tree at a constant distance and in a counterclockwise direction, finishing when the initial sub-grid, I , is found again, which means it is also in the final point, F [146]. An example of this method is illustrated in Figure 13b. The approximation depends on the side length, L , of the grid

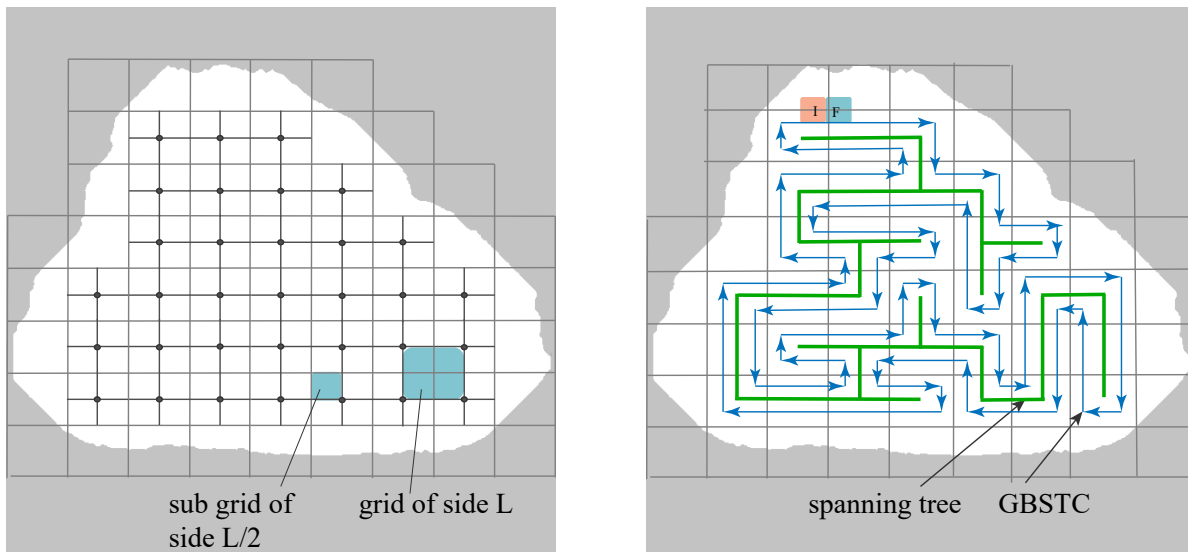


Fig. 13. a) Approximate cell decomposition in grids and sub grids. b), Coverage path generated with the GBSTC method.

c). *Grid-based Wavefront Coverage (GBWC)*: The first grid-based method proposed for CPP, GBWC is an offline method that uses a grid representation, in addition to applying a full CPP method. The method requires an initial grid, I , and a final grid, F . A distance transformation that propagates a wavefront from the final to the initial point is used to assign a specific number to each item on the grid. That is, the method first assigns a zero to the final item, and then a one to all its surrounding grids. Then all unmarked grids adjoining those marked one are numbered two. The process is incrementally repeated until the wavefront reaches the initial grid [147], as illustrated in Figure 14a.

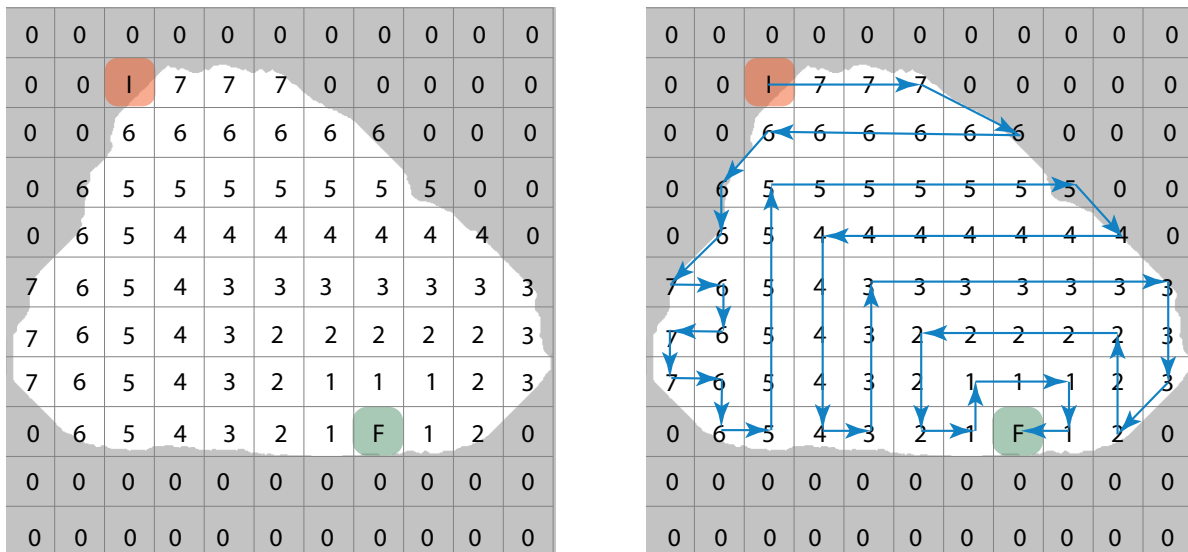


Fig. 14. a) Wavefront distance transform for the selection of the initial position (I), final position (F). b) Coverage path generated using the wavefront distance transform with the selection of the initial position (I).

Once the distance transformation is determined, a coverage path can be found by starting at the initial grid, I , and selecting the adjoining grid with the highest number that has not been explored. If two or

more are unexplored, and adjoining grids share the same number, one of them is randomly selected, as shown in Figure 14b.

d) Metrics

The metrics evaluate the performance of the three CPP methods. Such assessment can be performed by considering five commonly used metrics to evaluate the effectiveness of the proposed CPP methods both theoretically and in simulation (dynamically) [34], [48], [109], [111]. These five metrics are covered path length, flight time, energy consumption, redundancy of points traveled, and percentage of coverage of the total area. Each of these metrics is described below.

The L_{ct} metric (covered path length), is the length of the entire path covered by the UAV from the initial to the final point. For a trajectory in the 2D plane composed of n points, assuming the initial point as $(x_1, f(x_1))$ and the end point as $(x_n, f(x_n))$. The L_{ct} can be computed as shown in Equation (5):

$$L_{ct} = \sum_{i=1}^{n-1} \sqrt{(x_{i+1} - x_i)^2 + (f(x_{i+1}) - f(x_i))^2} \quad (5)$$

Where $(x_i, f(x_i))$, where $i = 1, 2, \dots, n$ are all the n points of the UAV flight path in the 2D coordinates. More details can be found in [148].

The flight time metric of the PX4 SITL Gazebo model is the time required to travel the total flight path (takeoff, path travel, and landing) with a dynamic speed that considers the inertia and the variation in speed due to UAV turns angles. These data are collected through sensors in the Gazebo plugins [149].

The redundancy of points traveled, $R_{\%}$, corresponds to the number of points that are visited more than once from the total number of points that the path contains, Equation (6).

$$R_{\%} = \frac{P_{pc}}{P_{vmo}} \quad (6)$$

where P_{pc} , and P_{vmo} correspond to the number of points the trajectory contains, and the number of points visited more than once [150].

Percentage of coverage of the total area $C_{\%}$, measures the number of effectively covered points within the total number thereof by the points the area to be covered contains, given by Equation (7).

$$C_{\%} = \frac{P_v}{P_T} \quad (7)$$

Where P_v and P_T correspond, respectively to the total number of points visited and the total number of points in the area [107].

Moreover, the number of maneuvers metric, which is the number of turning maneuvers the UAV performs on a path, is often used as the main performance metric in coverage [151], [152].

The energy consumption metric is computed from the voltage and current data from the power module of the PX4 SITL model [153]. Its value depends on parameters, such as the CPP width between lines and the speed and the height of the UAV at the time of implementing the CPP, which were configured in the interface and were simulated in Gazebo.

To validate the results of the methods described above, the BECD, GBSTC, and GBWC methods were implemented in two UAVs, simulated in Gazebo, and their performances were assessed by the metrics

presented above [107]. The next section describes the results and compares the models in detail.

4) *Simulation and Validation Platform:* Based on [154], the Gazebo platform was selected to execute the simulation experiments, as it has extensive documentation on its webpage. In addition, it is the most mentioned and used simulation platform in previous work [134], [135], that implemented path planning or CPP, used UAV sensors, or deployed several UAVs [154]. Gazebo also allows the modeling of commercial UAVs using the PX4 autopilot software [153], as shown in Figure 15. In addition, this figure shows one of the experiments conducted with the Typhoon UAV, flown over the CSUSL plant. The UAV sonar sensor, represented by blue lines, is also shown, as is the UAV camera, in the box at the upper right.

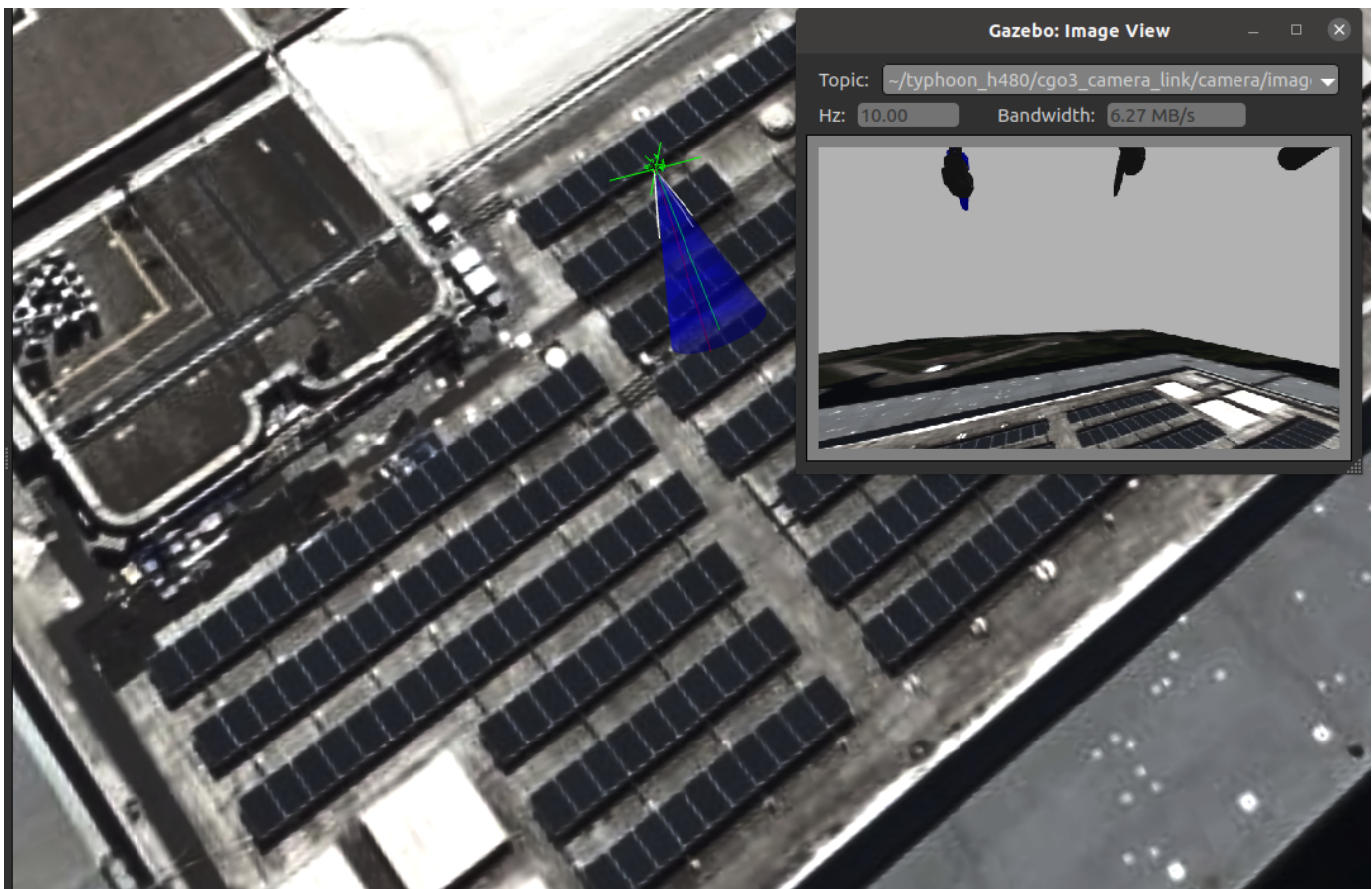


Fig. 15. UAV over the PV plant, simulated in Gazebo

The interaction between Gazebo [154], PX4 [153], Python and the CPP methods was implemented using ROS (Robot Operating System) as middleware [155]. This tool allows communication among nodes. The nodes are processes, and each node has a task associated with it, such as sending a Mavlink command to control the UAV trajectory and permitting reading messages from the UAV to discern its status in flight, using a simulation mode referred to as software in the loop (SITL). This simulator provides the ability to run different vehicles, such as a plane, copter, or rover, without a need for any microcontrollers or hardware [156]. In addition, two PX4 autopilot rotary wing UAVs, the 3DR Iris and Typhoon UAV, were chosen because they have good maneuverability and are more suitable for small-scale CPP missions. Furthermore, these UAVs have been widely used in other research [23], [131], [157].

The GCS software (QGroundControl) was selected to validate the CPP calculated for each UAV and PV plant obtained, because it is the most compatible tool with the PX4 autopilot. It is also recommended on the PX4 webpage. On other hand, another compatible tool, namely a GUI, was designed using Qt to modify and vary the parameters and to convert the way points from RoI pixels to geo-referenced points [61].

D. Results and Discussion

The procedure described above—DL-server, post-processing, CPP, and metrics evaluation, represented in Figure 11, was applied to three different PV plant images. The results obtained are described in the following sections.

1) *Results with Deep server and OpenCV functions:* OpenCV functions and a DL server were combined to accurately extract the mask and to trade off the DL server results of the PV plant area. Then, the CPP methods used the mask as a region of interest (RoI).

The stages to obtain the results of the RoI in the three images are shown in Figures 16–18. In the first stage, a high-resolution image from Google Maps, of predefined height and width, was obtained, and used as an input image in the DL server, depicted in Figure 16a. In the second stage, the output image of the DL server was the mask, shown in Figure 16b. In the third stage, the opening function was used in the mask, Figure 16c. In the fourth stage, the RoI was obtained using the draw contour method, as seen in Figure 16d. Finally, the RoI was blended with the input image with the aim of comparing the results in Figure 16e. The results were satisfactory and can be adapted, depending on the environment.

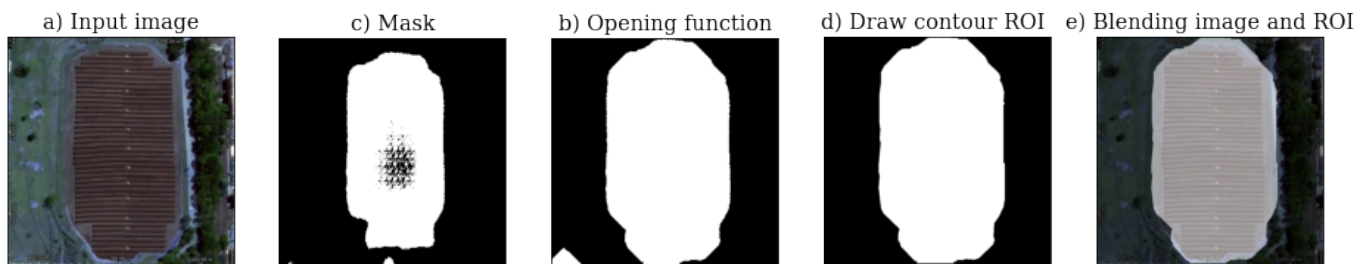


Fig. 16. Steps of boundary extraction by DL server and OpenCV functions in Unioeste 1 PV plant.

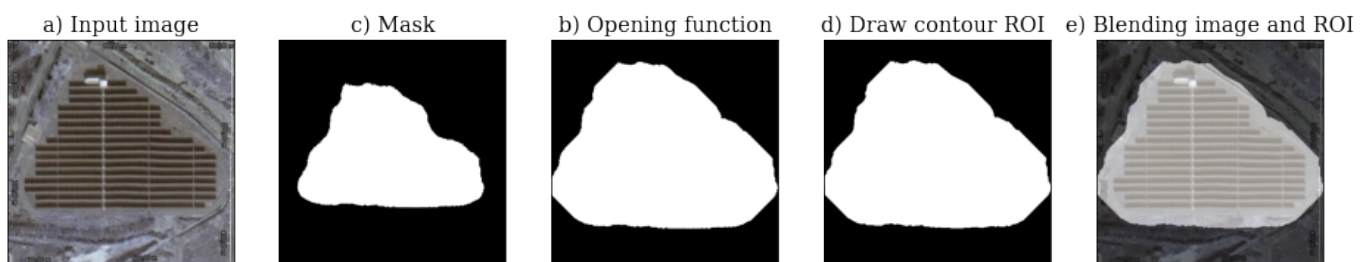


Fig. 17. Steps of boundary extraction by DL server and OpenCV functions in Arak PV plant.

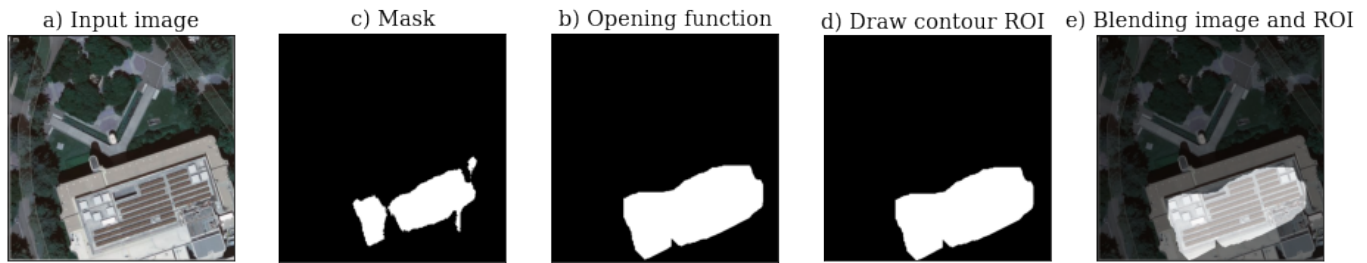


Fig. 18. Steps of boundary extraction by DL server and OpenCV functions in CSUSL PV plant.

2) *Results of CPP Methods:* The CCP method results were obtained from six experiments that implemented the five metrics previously described. Each experiment was conducted by selecting a PV plant and a UAV, then choosing the CPP method and the width, speed, and height of the UAV over the flight path. All of this was done in the implemented GUI interface. The six tests were conducted by varying the CPP width parameter, while other parameters were not varied, and the same experimental conditions were maintained throughout.

For these experiments two UAVs were selected, the Typhoon [158] and 3DR Iris [159] as mentioned in Section 4. Three simulated PV plants were also chosen, as highlighted in Section C. The metrics referenced in Section 3 were assessed for each test. Battery consumption was obtained from the GCS software with the SITL parameter activated. The rest of the data was collected from the Gazebo simulations. The experiments are explained in detail in the following sections, and some results are discussed.

a) *The Three First Experiments with a Typhoon UAV*

The three first CPP experiments were conducted with a Typhoon UAV, varying the CPP width between 0 and 20 m, depending on the PV plant being covered. For example, in the first and second PV plants, Unioeste 1, and Arak, respectively, the CPP widths were varied between 5 and 20 m. In the third CSUSL PV plant, the width was varied between 1 and 8 m, due to the method's restrictions on running in small areas with a large width. Then, in each of these experiments, the resulting metrics were annotated in Tables, as shown in Appendix B.

The logged metrics were utilized to draw a clustered columns and lines chart for experiments 1, 2 and 3, performed with the Typhoon UAV, to highlight the most important information and to determine their correlations with each other. In these graphs the vertical axis was scaled logarithmically and the horizontal axis was labeled with the type of CPP method in use; in this way, it is possible to visualize the correlation of flight time, number of maneuvers, and covered path length with the energy consumption by each CPP method, as shown in Figures 19–21. In addition, the relationship between the redundancy metric and the CPP width is identified, showing that this metric is higher in BECD, but does not affect energy consumption, which is the primary metric of interest.

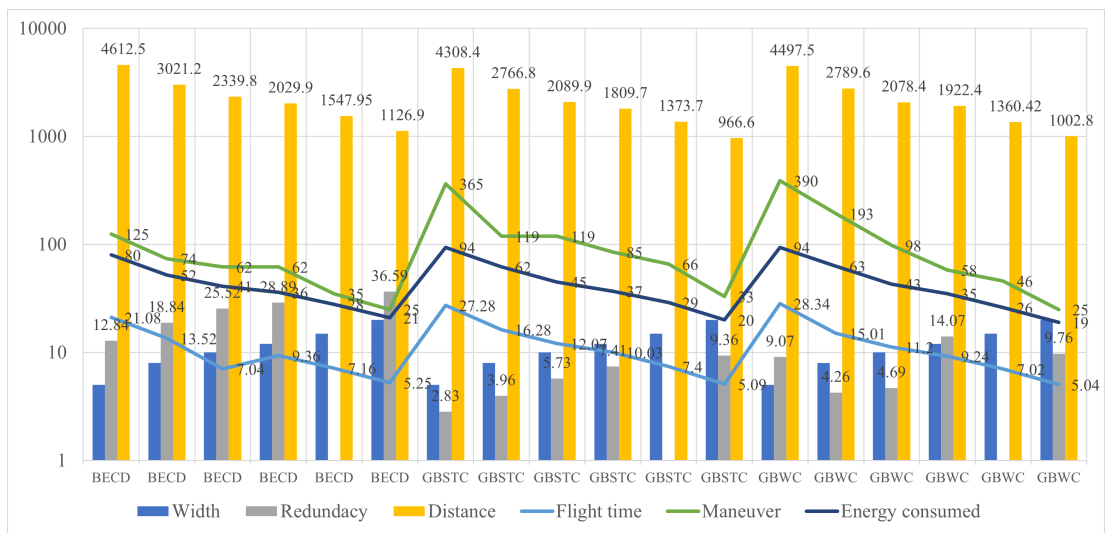


Fig. 19. Performance metrics of Typhoon UAV on Unioeste PV plant (Experiment 1).

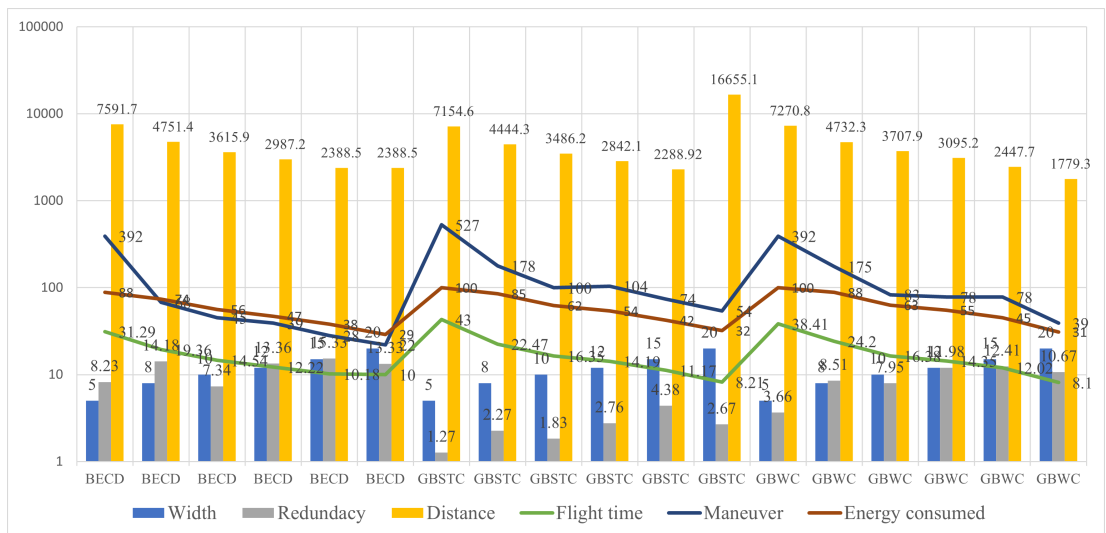


Fig. 20. Performance metrics of Typhoon UAV on Arak PV plant (Experiment 2).

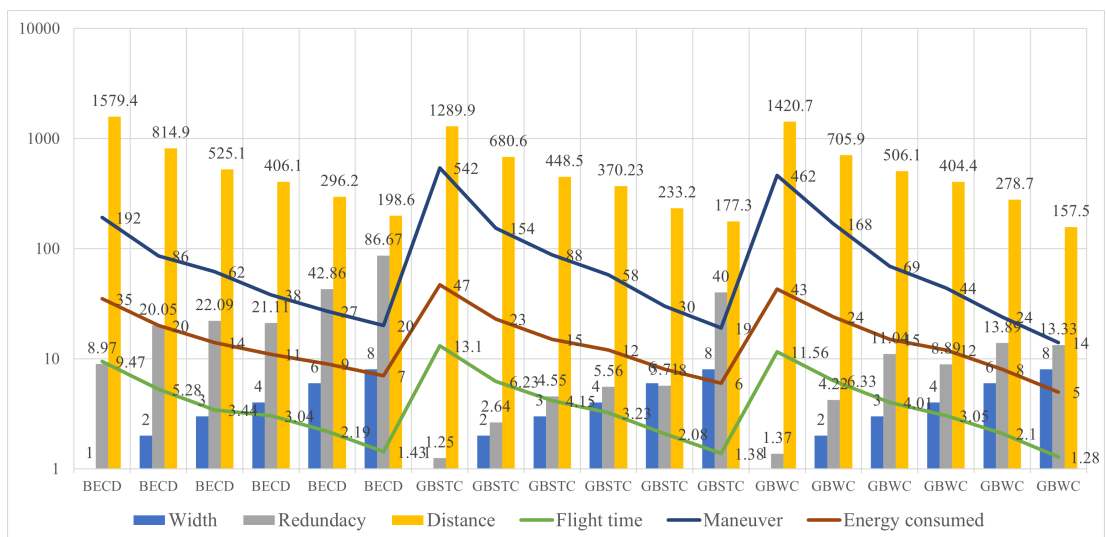


Fig. 21. Performance metrics of Typhoon UAV on CSUSL PV plant (Experiment 3).

The UAVs' energy consumption, in conjunction with the CPP widths, were obtained from the energy consumption results logs, then a new Table V was composed of three large columns, corresponding to all the assessed PV plants, and each PV plant column is made up of three CPPs with their respective values of consumed energy. The rows of the table contain the CPP widths in increasing order from top to bottom, as shown in Table V. Where it can be observed, some parameters, such as the energy consumption with regard to CPP width, were due to the size of the RoI. Additionally, it can be observed that the greater the CPP width, the lower the energy consumption, as seen in the columns of Table V. For example, for the BECD CPP in Unioeste 1, with a width of 5 m, the percentage of energy consumed was 98%, while, for a width of 20, the energy consumed was 29%. It is also observed that the larger the PV plant, the UAV consumed all its energy in CPPs with narrow widths; on the other hand, if the plant is small, with the same width, the UAV does not have energy consumption problems. As can be seen in the row with a width of 8 m, where, for the Unioeste 1 and Arak PV plants, a lot of energy was consumed, between 88% and 52%, unlike the CSUSL plant, in which where the energy consumed was very little, between 7% and 5%. In the experiments for which energy consumption, with respect to CPP width, cannot be observed, (*N/A*) was used to annotate these results, which happened when the CPP width was very large with respect to the RoI, as this does not allow the generation of the route, or when the CPP width was very small with regard to the RoI causing a flight path in which the UAV consumes all its energy. In short, the UAV used can be undersized or oversized with respect to its intended PV plant.

TABLE V. COMPARISON OF THREE CPP METHODS WITH RESPECT TO THE CPP WIDTH, SIMULATED IN A TYPHOON UAV ON THREE PV PLANTS

PV plant	Energy Consumption								
	Unioeste 1 (35,975m ²)			Arak (25,056m ²)			CSUSL (1,344m ²)		
	BECD	GBSTC	GBWC	BECD	GBSTC	GBWC	BECD	GBSTC	GBWC
CPP Width (m)									
1	<i>N/A</i>	<i>N/A</i>	<i>N/A</i>	<i>N/A</i>	<i>N/A</i>	<i>N/A</i>	35%	47%	43%
2	<i>N/A</i>	<i>N/A</i>	<i>N/A</i>	<i>N/A</i>	<i>N/A</i>	<i>N/A</i>	20%	23%	24%
3	<i>N/A</i>	<i>N/A</i>	<i>N/A</i>	<i>N/A</i>	<i>N/A</i>	<i>N/A</i>	14%	15%	15%
4	<i>N/A</i>	<i>N/A</i>	<i>N/A</i>	<i>N/A</i>	<i>N/A</i>	<i>N/A</i>	11%	12%	12%
5	98%	100%	100%	80%	94%	94%	<i>N/A</i>	<i>N/A</i>	<i>N/A</i>
6	<i>N/A</i>	<i>N/A</i>	<i>N/A</i>	<i>N/A</i>	<i>N/A</i>	<i>N/A</i>	9%	8%	8%
8	74%	85%	88%	52%	62%	63%	7%	6%	5%
10	56%	62%	63%	41.5%	45%	43%	5%	<i>N/A</i>	5%
12	47%	54%	55%	36%	37%	35%	<i>N/A</i>	<i>N/A</i>	<i>N/A</i>
15	38%	43%	45%	27%	29%	26%	<i>N/A</i>	<i>N/A</i>	<i>N/A</i>
20	29%	32%	31%	21%	20%	19%	<i>N/A</i>	<i>N/A</i>	<i>N/A</i>

The graphs in Figure 22 were constructed from Table V by quintic polynomial interpolations, which requires six data points to form a curve that passes through all given data points [160], where the abscissa axis is the CPP width and the ordinate axis is energy consumption. For the experiment conducted at the PV plant Unioeste 1, the graph in Figure 22a shows that the BECD method had the lowest energy consumption when the CPP width was in the range of 5 to 16 m, while GBSTC and GBWC had the

lower energy consumption when the CPP width was in the range of 16 to 20 m. For the experiment tested at the Arak PV plant, the graph in Figure 22b shows that the BECD method had the lowest energy consumption when the CPP width was in the range of 5 to 10 m, while the GBSTC and GBWC had similar energy consumption when the CPP width was in the range of 10 to 15 m, and GBWC had the lowest energy consumption when the CPP width was in the range of 15 and 20 m. For tests conducted at the CSUSL PV plant, the graph in Figure 22c shows that the BECD method had the lowest energy consumption when the CPP width was in the range of 1 to 5.5 m, while the method GBSTC had the lowest energy consumption when the CPP width was in the range of 5.5 to 8 m. All plants were recreated in a simulation environment with their real dimensions.

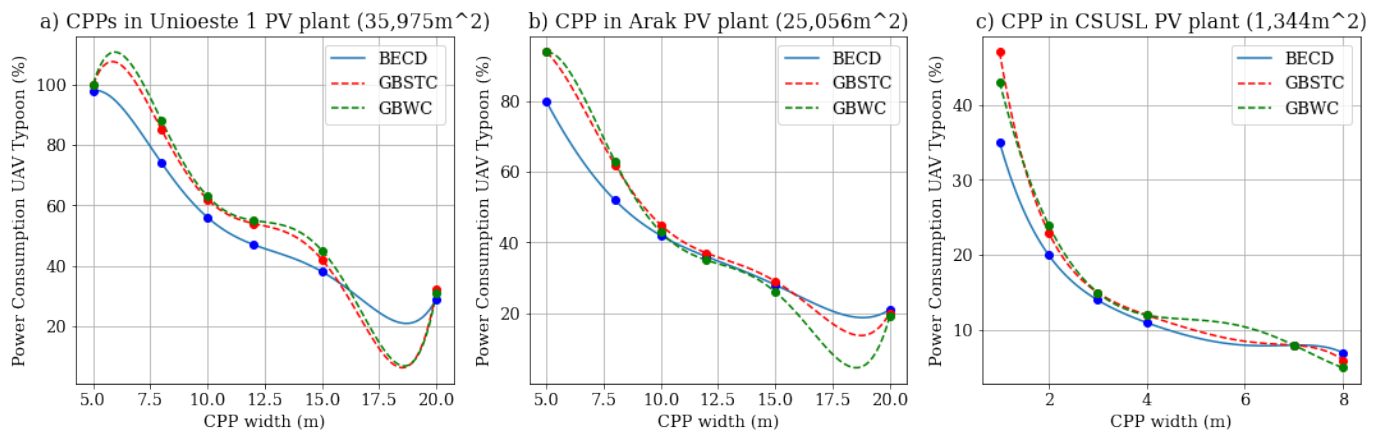


Fig. 22. Performance test of UAV Typhoon varying the CPP width.

The Last Three Experiments with 3DR Iris UAV

The last three CPP experiments were conducted with a 3DR Iris UAV, varying the CPP width between 1 and 20 m, depending on the PV plant covered. For example, in the first and second PV plants, Unioeste 1 and Arak, respectively, the CPP widths were varied between 8 and 20 m; in the third PV plant, CSUSL, the width was varied between 1 and 8 m, due to the restrictions of the method requiring it be run in small areas with a large width. Then, in each of these experiments, the resulting metrics were annotated in tables, as shown in Appendix C.

As in the previous chapter, the recorded metrics were used to create bar and line graphs for Experiments 4, 5 and 6, which are those conducted with the 3DR Iris UAV, to highlight the most important information and to determine correlations among the metrics. In these graphs, the vertical and horizontal axes were scaled logarithmically and labeled in the same manner as above, with the aim of visualizing the correlations between flight time, number of maneuvers and covered path length, with regard to energy consumption by each CPP method, as shown in Figure 23–25. Furthermore, the relationship between the redundancy metric and CPP width is identified, showing behavior similar to the previous UAV's data.

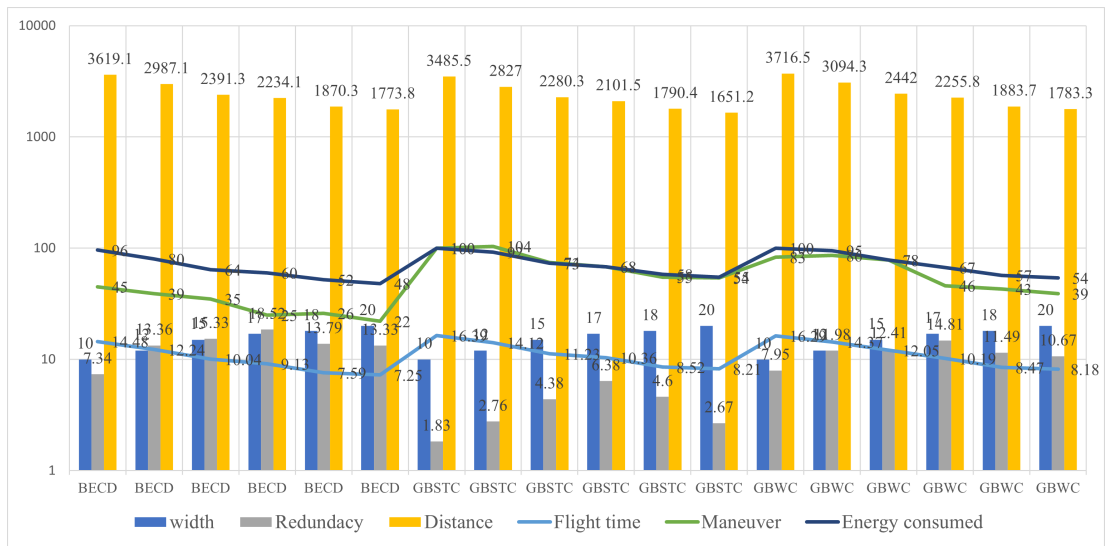


Fig. 23. Performance metrics of 3DR Iris UAV on Unioeste PV plants (Experiment 4).

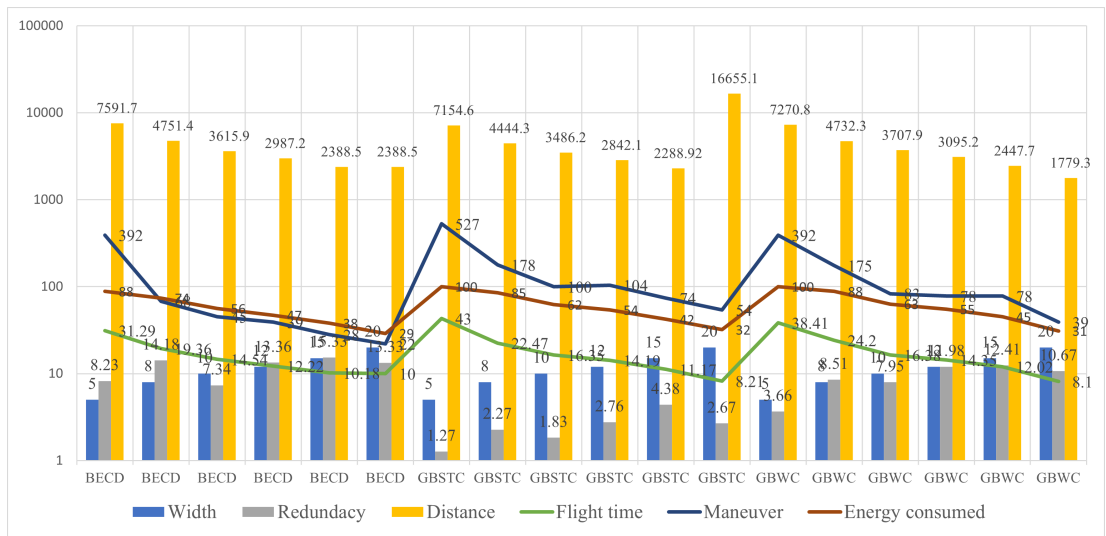


Fig. 24. Performance metrics of 3DR Iris UAV on Arak PV plants (Experiment 5).

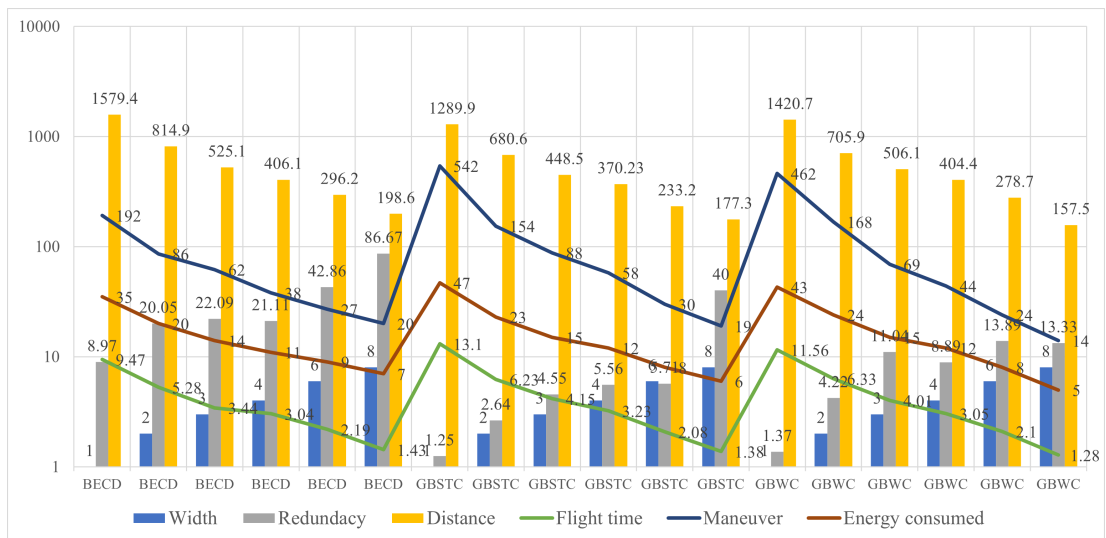


Fig. 25. Performance metrics of 3DR Iris UAV on CSUSL PV plants (Experiment 6).

The UAV energy consumption and CPP widths were obtained from the energy consumption results logs, then a new Table VI was established, in which three large columns correspond to the PV plants, where each PV plant column contains three CPPs with their respective values of consumed energy, and the rows of the table contain the CPP widths in an increasing direction from top to bottom. Here it can be observed, as in the last table, that some parameters' values, such as the energy consumption by CPP width, are due to the size of the RoI. It can also be observed that the greater the CPP width, the lower the energy consumption, as seen in the columns of Table VI. For example, using BECD at Unioeste 1 with a width of 10 m, the percentage of energy consumed was 100%, while for a width of 20 m, the energy consumed was 48%. It is also observed that, for larger PV plants, the UAV consumed all its energy in a CPP with a small width, whereas, for small plants of the same width, the UAV did not have energy waste problems. As can be seen in the row corresponding to a CPP width of 8 m, at the Unioeste 1 and Arak plants a lot of energy was consumed, between 100%, and 88%, unlike at the CSUSL plant, where the energy consumed was very little, between 9%, and 8%. Similarly, in the previous experiments, wherein the UAV's energy was exhausted and the CPP width did not allow the generation of the route or when the CPP width was large with regard to the RoI, the results were scored with (*N/A*). To summarize, the UAV used is suitable for the last PV plant.

On the other hand, the 3DR Iris UAV, with its design, size, autonomy, and performance is suitable when the PV plant to be inspected is small, of an approximate size of 5000 square meters or less, such as the CSUSL PV plant, at 1344 square meters. Owing to such PV plant sizes, any coverage method used in this work can be used to cover an area with a CPP width of 1 meter, while minimizing the metrics of covered path length, flight time and maneuverability, to obtain lower energy consumption, as shown in the Table VI. In addition, this UAV did not perform well at large or medium-sized plants, since, to cover them using the CPP method, the width that must be provided is greater than 8 m; therefore, though the UAV's inspection of the PV plant had no high-resolution cameras on board, they were needed; without them, the inspection cannot be guaranteed.

TABLE VI. COMPARISON OF THREE CPP METHODS WITH RESPECT TO THE CPP WIDTH, SIMULATED IN A 3DR IRIS UAV ON THREE PV PLANTS

PV plant	Energy Consumption								
	Unioeste 1 (35,975m ²)			Arak (25,056m ²)			CSUSL (1,344m ²)		
CPP Width (m)	BECD	GBSTC	GBWC	BECD	GBSTC	GBWC	BECD	GBSTC	GBWC
1	N/A	N/A	N/A	N/A	N/A	N/A	52%	72%	72%
2	N/A	N/A	N/A	N/A	N/A	N/A	30%	35%	38%
3	N/A	N/A	N/A	N/A	N/A	N/A	21%	24%	22%
4	N/A	N/A	N/A	N/A	N/A	N/A	17%	17%	15%
5	N/A	N/A	N/A	N/A	N/A	N/A	N/A	N/A	N/A
6	N/A	N/A	N/A	N/A	N/A	N/A	12%	12%	11%
8	100%	100%	100%	88%	98%	98%	9%	9%	8%
10	96%	100%	100%	70%	76%	71%	7%	N/A	7%
12	80%	92%	95%	60%	63%	59%	N/A	N/A	N/A
15	64%	73%	78%	45%	48%	43%	N/A	N/A	N/A
17	60%	68%	67%	N/A	N/A	N/A	N/A	N/A	N/A
20	48%	55%	54%	26%	26%	25%	N/A	N/A	N/A

The graphs in Figure 26 were constructed from Table VI using quintic polynomial interpolations, wherein the abscissa axis is CPP width and the ordinate axis is energy consumption.

Additionally, the graph in Figure 26a shows that the BECD method had the lowest energy consumption; when the CPP width spanned the entire test range, the GBSTC and GBWC methods showed a higher energy consumption at the Unioeste 1 PV plant. The graph in Figure 26b shows that the BECD method had the lowest energy consumption when the CPP width was in the range of 8 to 10 m, whereas BECD and GBWC had similar energy consumption, leaving the GBWC method with the lowest consumption, when the CPP width was in the range of 10 to 15 m. On the other hand, the GBWC method had the lowest energy consumption when the CPP width was in the range of 15 and 20 m; this test was conducted at the Arak PV plant. Finally, the graph in Figure 26c shows that the BECD method had the lowest energy consumption when the CPP width was in the range of 1 to 3 m, and the GBWC method had the lowest consumed energy when the CPP width was in the range of 3 to 8 m. The test was performed at CSUSL's PV plant.

Summary Tables of the results of the metrics for each of the tests with the Typhoon UAV and 3DR Iris UAV are shown. All files, and logs for the experiments are available on GitHub at [161].

3) *Discussion:* The proposed strategy allows a semi-automatic and faster solution for achieving effective results when inspecting PV plants in geometrically simple areas, with certain limitations, although some results obtained in this work are theoretical results, such as from CPP width, for example; in practice, a camera of 14 megapixels is not adequate to inspect a PV plant with a CPP width of 20 m [46], [162]. The results obtained in this work indicate that the most adequate method is BECD for a specific range of CPP widths, although it also shows adequate performance for various CPP widths in some RoIs. The

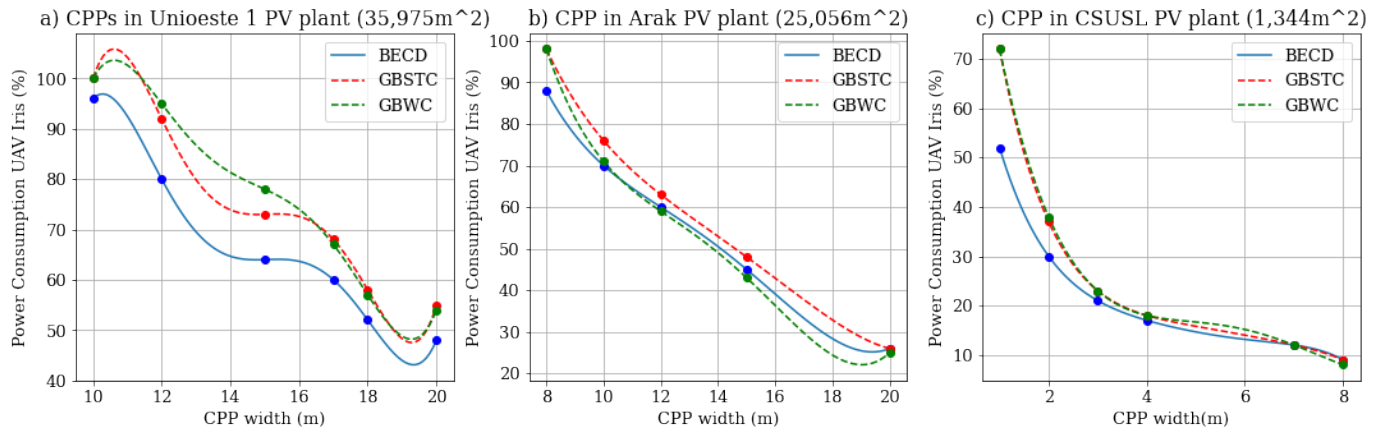


Fig. 26. Performance test of UAV 3DR Iris varying the CPP width.

GBWC showed a good performance when using a CPP width greater than 7 m in some RoIs, and all showed a relationship with the area to be covered, as shown in Tables V and VI.

An analysis of the metrics used in this work, such as redundancy, $R\%$, which does not represent a significant factor when comparing these three CPP methods, showed that, although the BECD was the method with the highest redundancy, it was also the method with the lowest consumption of energy. On the other hand, the other metrics, such as the L_{ct} metric, flight time metric, and the number of maneuvers, are directly related to energy consumption, as can be seen in Appendix B and C. It also helps to conclude that the BECD method is more suitable for widths in a range between 0 and 7 m, due to the lower number of maneuvers in these ranges, as other authors have also mentioned [163], [164]. The percentage of coverage of the total area, $C\%$, always showed that coverage was total

The L_{ct} metric, flight time and number of maneuvers were directly related to the consumption of energy for all the experiments performed, as seen in Figures 19–21 and 23–25, and as confirmed by other authors [151], [152], in addition to helping to reinforce that the most appropriate CPP for certain ranges is the BECD.

The BECD method is the best method among the three methods tested, in a specific width range, from 0 to 7 m, for all the RoIs tested, which means that for a 10 Megapixel camera with a horizontal field of view of 7 m, the CCP method's good images, in terms of what to inspect of a PV plant can be obtained [33].

The implemented BECD method divided the RoI into small regions, and then, over these regions, it implemented the round-trip coverage pattern, called boustrophedon [106], [107]. This pattern allows spending less energy consumption with small widths, due to its low number of maneuvers compared with the other methods, as shown in Appendix B and C.

On the other hand, the GBWC method allowed lower energy consumption, according to the results of the simulations, in widths greater than a certain value, but depending on RoI size; this method also allows an approximate coverage outside the RoI, a characteristic that is very important in this type of application, and that, perhaps, is not very attractive for terrestrial robotics, from which this type of method originates [147].

A RoI with many concave points is a great challenge for performance metrics, since they increase

with the distance of travel, and also increase the number of maneuvers and therefore increase energy consumption, according to these results in the following works [23], [164], a more detailed analysis on these characteristics was made.

In future works, the methods (BECD, GBWC) could be implemented in UAVs with characteristics similar to those used in this work; these characteristics are shown in Tables VII and XI. Additionally, with these UAVs, an inspection could be conducted in at least one PV plant. Where one can think about the implementation of an expert system that selects the coverage path between the two types of methods (BECD, GBWC), according to the CPP width size, required for a camera with a certain resolution, and focal length.

Finally, the results obtained with the BECD, and GBWC methods differ from the results obtained by other authors [46], [103]–[105]. Who did not implement CPPs to solve these types of problems; they used other types of solutions that have restrictions when inspecting PV plants with UAVs. On the contrary, this work considers the CPPs, and obtained interesting results for future real implementation. The proposed CPP will increase the possibility of using inexpensive UAV systems for the inspection of PV systems on roofs of houses, and commercial buildings, and also, of the use of CPP with small widths to complete inspections at centimeter scales of the panel where the flaws can be better seen.

E. Conclusions

In this work, a method for implementing CPP in UAV for PV plant inspection was presented. The method consisted of a series of steps, one of these was the deployment of a DL-based U-net model to establish a DL service system from which to extract the limits of PV plants by extracting the boundaries of PV plants from an image. To summarize, the method was accurate, and fast without depending on the image, with low request latency and response.

This experiment focused on three novel path planning methods in the PV inspection missions in order to find the best path for covering each of the three PV power plants with less energy consumption. A GUI interface was used to order the UAV's maneuvers in the inspection of the simulated PV plants. The results of each CPP method in the simulation were compared. The best CPPs was the BECD, for a range of CPP widths of 0 to 7 m. These path planning algorithms can be performed by any multirotor UAV that receives Mavlink commands, can carry a camera sensor, and transmit real-time video to GCS.

Performance on the CPP tasks was measured using two different types of flying robots, a Typhoon UAV and a 3DR Iris UAV. It was demonstrated that the Typhoon UAV (or one with similar characteristics) is better suited for large or medium-sized PV plants (such as those in deserts, plains, and hills); instead, the drone-like 3DR Iris UAV is more suitable for small-sized PV generation (such as on roofs and rooftops, canopies, and facades). The proposed strategy allows such comparisons to be made and enables the selection of the most suitable UAV for each type of installation.

The values obtained for the metrics collected from each of the tests show a correlation between covered path length, flight time, number of maneuvers as regards energy consumption, and ensuring that the CPPs implemented in UAVs to inspect photovoltaic plants could be similar when implemented in real plants. The

results also help to predict the energy consumption of a given UAV when performing a plant inspection.

VII. RESULTS AND DISCUSSION

A. *abstract*

This chapter presents a summary of the results obtained and the scope developed from the general objective of this work, which was to propose a strategy to determine the coverage route in unmanned aerial vehicles, from a delimitation of photovoltaic installations through image analysis and in a suitable simulation environment, for a future inspection of solar panels. and to achieve this objective, three specific objectives were proposed and developed in a modular way in two stages. Where satisfactory results were obtained that achieved a great contribution in the state of the art, such as a technique to delimit geometric area of photovoltaic plants, a CPP technique that is suitable for the task in a range of specific CPP widths and the implementation of the entire system with a GUI interface and a simulation platform, to select different photovoltaic plants and drones where the system was put into operation and through these experiments a series of recommendations for implementation of a system, were obtained. Thus fulfilling the specific objectives and the general objective.

keywords: deep learning (DL); unmanned aerial vehicle (UAV); photovoltaic (PV) plants; semantic segmentation; coverage path planning (CPP).

B. *Introduction*

The main objective of this work was to propose a strategy to determine the coverage flight path in unmanned aerial vehicles, based on a boundary mapping of photovoltaic plants through image analysis and in a suitable simulation environment, for a future inspection of solar panels.

To achieve this goal, a series of specific objectives per stage were proposed. In the first stage, the proposed objective was to evaluate image processing techniques for the extraction of the area limits of a photovoltaic plant. In the second stage, the proposed objective was to specify a method for planning coverage routes over the area of photovoltaic installations. The last proposed objective was to evaluate the performance of the system in the simulation environment, verifying its operation on at least two PV installations and creating a set of recommendations for system deployment based on a simulation environment.

In two stages several results were found, each of which will be explained in the following paragraphs and additionally the scope developed and achieved in the work will be explained.

C. *Summary results and scope of work*

1) *Primera Etapa:* In the first stage, as a result of the first specific objective, several contributions were achieved: the first one was the selection of the "Amir" dataset among many others, through a process of database specification, where the main characteristics on which the selection of the dataset was based

were: that the images of the photovoltaic plants had their respective masks and that they had low resolution to facilitate the training of the neural network.

As a result of this objective, several contributions were achieved: the first was the search and selection among many options of the "Amir" dataset, this was done through a process of database specification, where the main characteristics on which the selection of the dataset was based were: that the images of the photovoltaic plants had their respective masks and that they had a low resolution to facilitate the training of the neural network.

Secondly, the values obtained in this work with the TIP technique and those obtained by other authors were compared. This process was carried out by randomly selecting test images and applying the functions described in the methodology section, and then comparing the mask obtained with the original. The comparison of the obtained mask with the original one gave the following results: for the IoU metric it was 71.62% and DC was 71.62%. The results were accurate and can be modified depending on the environment.

Third, a comparison was made between the results obtained with the TIP technique and the deep learning techniques (the FCN model [32] and the proposed U-net model). To perform this comparison, the two most commonly used metrics in semantic segmentation problems were used. For example, for the implemented FCN model the result of the standard IoU metric in the training stage was 94.13%, for the validation stage it was 90.91% and for the test stage it was 87.47%. In addition, in the DC metric in the training stage it was 95.10%, for the validation stage it was 92.96% and for the test stage it was 89.61%, which have similar values. On the other hand, using the same metrics of the proposed U-net model, it is found that the IoU metric obtained in the training stage was 93.57%, in the validation stage 93.51% and in the test stage 90.42%. Likewise, the DC metric for the training stage was 94.03%, for the validation stage it was 94.44% and for the test stage it was 91.42%. Due to this, a large difference was found between the TIP models and the DL-based models, a not so marked difference between the FCN and U-net model for the first metric of 2.95% in the testing stage and for the second metric used a difference of 1.81% was calculated in the same stage, resulting in a better performance in the metrics of the U-net model of Deep Learning.

Finally, the general trend of the FCN model behavior during the training and validation stage is consistent, showing that the network converges and is stable at iteration 30, and the loss value tends to 0.04%. On the other hand, for the U-net model proposed in this work showed a better performance. The common trend of the two metrics and the network, converges in less time and is stable at iteration 16, the loss value tends to 0.03%. Having less loss and therefore higher performance.

To sample the above inputs, 716 images with the FCN model and the trained U-net model were used in the evaluation stage, where the U-net model shows better performance when comparing the FCN model test data. As shown in Figure 9 and 10, For example, in one of the images showing a photovoltaic plant and a lake, the U-net model differentiates between the lake and the photovoltaic plant, which is not the case with the FCN model.

The training and testing accuracy is a proportion of the number of pixels from the original image that are correctly classified in the predicted image and this cannot be taken as indicators of the similarity between the predicted PV plants and the original mask for the semantic segmentation task [85].

To confront the results of the original and the predicted mask, the IoU metric was used. This metric varies from 0 to 1, with 0 being the lack of similarity and 1 being the complete similarity between the masks [82], so the U-net model proposed in this work obtained a value closer to 1 in the IoU metric. In addition, the iteration times show that the model used is faster and therefore reliable for the training and processing stages, obtaining results in less time [85]. As a result, the U-net model performed better compared to the FCN model, allowing the specific objective of the first stage to be met.

2) *Second Stage (Objective 2 and 3):* In the second stage, the specific objective is to specify a method for planning coverage routes over the geometric area of photovoltaic installations.

In the literature on CPP, several methods have been used to solve the CPP problem. In this work, three methods based on CPP were selected, considering the following criteria: execution time, ease of implementation and easy understanding, which were used to cover the RoI. The methods were selected according to [106], [107]. These three methods were: Boustrophedon exact cellular decomposition (BECD), grid-based spanning tree coverage (GBSTC), which works with cellular decomposition, and grid-based wavefront coverage (GBWC).

In addition, the environment of the CPP work was mapped using Deep Learning Server and combined with OpenCV functions to extract the mask of the PV plant more accurately and to compensate for any incompatibility that the result could present with the region of interest (RoI) required by the CPP methods. As verified in the last part of this process, where the RoI was blended with the input image in order to compare the results, they were satisfactory and could be automatically adapted according to the environment.

The CCP methods were evaluated with five metrics (path length covered, flight time, energy consumption, redundancy of points traveled and percentage coverage of the total area) dynamically in six experiments that were implemented in a simulation environment, each experiment was configured by selecting one PV plant out of three possible, one UAV out of two possible, one CPP method out of three possible, one speed, one UAV height above the flight path and only the CPP width was varied for one configuration, i.e. 6 variations for each configuration, for a total of 108 simulated runs, all of the above was performed in the implemented GUI interface.

From the experiments with the CPP methods, some contributions were obtained, i.e., it is possible to specify the most suitable CPP in terms of the metrics that directly influence the energy consumed to meet the second specific objective, i.e., the results obtained in this work indicate that the most suitable method is BECD for a specific range of CPP widths from 0 to 7 meters, although it also shows adequate performance for several CPP widths in some RoIs. On the other hand, the GBWC method showed good performance when using a CPP width greater than 7 meters in some RoIs.

Continuing in the second stage, the third specific objective consisted of evaluating the performance of the system in the simulation environment, verifying its operation in at least two PV installations and creating a set of recommendations for implementing the system based on the results of the simulation environment. The same six experiments of the second stage were used, but the behavior of the selected plants and UAVs were analyzed, for these experiments two UAVs were selected, the Typhoon [157] and the 3DR Iris [158] widely used in research works, also three simulated photovoltaic plants were chosen (Unioeste, Arack, and

CSUSL) , where were evaluated for each test, the battery consumption and metrics performance where it was found that the best UAV to perform the Inspection task in small plants is the 3DR Iris based, also the inspection task was evaluated with the Typhoon, which presented a better performance in medium or large size plants.

On the other hand, based on the results obtained in the simulation and considering that the objective of the overall project is to implement the system in plants located on terraces and roofs, according to the result of the evaluation of simulated photovoltaic plants, the UAV to be used would be the 3DR Iris, with a low resolution camera.

Finally, thanks to the experimental analysis and the simulation environment used, it is considered that other projects of this research group can be supported by this work, some ideas are presented here:

- Swarm flight: start implementing other quadcopters with the same structure, in the same simulation environment to work on the interaction between several UAVS and the GCS ground station, thus achieving a faster inspection of medium and large PV plants.
- Integration of the video stream: the real-time video stream can be integrated into the design to be processed by another more up-to-date convolutional neural network structure, identifying problems in the PV plants in real time and being able to solve some problems immediately.
- In future work, an automatic flight controller on the PX4 Platform with Pixhawk brand hardware and a computer (Raspberry Pi) could be implemented on the UAV board to perform automatic flight and semantic segmentation of images on the same device.
- Currently there are many projects in development with the PX4 platform that are commercializing these devices that are open platforms that do not present restrictions for communication and interaction, therefore they can be used for future developments, as it has a large support community.

VIII. GENERAL CONCLUSIONS

To conclude, after evaluating traditional image processing techniques and artificial vision techniques that allow identifying and delimiting the area of PV installations from previously established images, it is possible to find based on metrics that the best method to solve this task it is with CNN, in particular with the U-net model.

In summary, after specifying a method of planning coverage routes on the geometric area of the previously identified PV installations, it is possible to identify two candidates of the valued, as the most suitable for the inspection task, but for time and resources it would be ideal try all the methods that exist in the state of the art, to compare and obtain the most optimal CPP according to the different parameters such as cpp width, energy consumed, geometry and size of the PV plant, etc.

In conclusion, when evaluating the system in a simulation environment, its operation was verified in at least three PV installations, and it was possible to create a set of recommendations to implement the real system based on the results obtained in the simulation environment.

This study characterized the different most common coverage path planning methods with UAVs applied to the operation and maintenance of PV plants at any location. The characteristics evaluated were speed, height, width between lines of the CPP. This characterization allowed the identification of width patterns between CPP lines with respect to power consumption, with constant height and speed, but varying the coverage areas. As expected, there is a relationship between the observed data, the inspections with small widths in large areas of PV plants require large amounts of energy.

APPENDIX A
ALGORITHM

Algorithm 2: OpenCV functions.

```

1. input : A image  $I_r$  of size  $w \times l$ 
2. output: A Map for robot
3. initialization
4. import cv 2, np, flask, tensorflow, matplotlib
5. do
6.    $lm \leftarrow cv2.imread(Mask)$ 
7.    $th \leftarrow cv2.Threshold(I_m, 128, 255, THRESH_BINARY, THRESH_OTSU)$ 
8.    $k \leftarrow cv2.getStructuringElement(MORPH_RECT, (1, 1))$ 
9.    $j \leftarrow cv2.getStructuringElement(MORPH_RECT, (5, 5))$ 
10.   $lerosion \leftarrow cv2.erode(th2[w, l], k, iteration = 2)$ 
11.   $ldilation \leftarrow cv2.dilate(lerosion[w, l], j, iteration = 20)$ 
12.   $ThImage \leftarrow ldilation.astype(np.uint8)$ 
13.   $cnt \leftarrow cv2.findContours(ThImage[w, l], RETRE_XTER, CHAIN_APX_NONE)$ 
14.  for  $i$  in  $cnt$ :
15.     $area \leftarrow cv2.contourArea(cnt)$ 
16.    if  $(area > 400)$ :
17.       $apx \leftarrow cv2.approxPolyDP(cnt, 0.0010 * cv2.arcLength(cnt, True), True)$ 
18.       $cv2.drawContours(image\_copy, [apx], -1, (0, 0, 255), 7)$ 
19.   $mask \leftarrow cv2.zeros([w, l])$ 
20.   $cc \leftarrow cv2.drawContours(mask, cnt, -1, (255, 255, 255), -1, FILLED)$ 
while  $True$ 

```

APPENDIX B
TABLES OF TYPHOON

TABLE VII. YUNEEC UAV TYPHOON TECHNICAL SPECIFICATION


UAV Typhoon	
	
Dimensions	520 x 457 x 310 mm (20,5 x 18 x 12,2 inches)
Weight	1980 g (69,8 ounces)
Battery	5400 mAh 4S/14,8 V (79,9 Wh)
Camera	12.4 Megapixels, 14mm/F2.8
Flight Time	Up to 25 min
Flight Speed	20o m/s
Payload Capacity	10.400 g
Motor	AC YUNH520120

TABLE VIII. THREE CPP METHODS USING TYPHOON UAV OVER UNIOESTE 1 PV PLANT (EXPERIMENT 1).

width	CPP	Redundacy	Distance	Travel time	Maneuver	Bat Conspt
5	BECD	8.23	7591.7	31.29	392	88
8		14.18	4751.4	19.36	68	74
10		7.34	3615.9	14.54	45	56
12		13.36	2987.2	12.22	39	47
15		15.33	2388.5	10.18	28	38
20		13.33	2388.5	10	22	29
5	GBSTC	1.27	7154.6	43	527	100
8		2.27	4444.3	22.47	178	85
10		1.83	3486.2	16.35	100	62
12		2.76	2842.1	14.19	104	54
15		4.38	2288.92	11.17	74	42
20		2.67	16655.1	8.21	54	32
5	GBWC	3.66	7270.8	38.41	392	100
8		8.51	4732.3	24.2	175	88
10		7.95	3707.9	16.38	83	63
12		11.98	3095.2	14.35	78	55
15		12.41	2447.7	12.02	78	45
20		10.67	1779.3	8.1	39	31

TABLE IX. THREE CPP METHODS USING TYPHOON UAV OVER ARACK PV PLANT (EXPERIMENT 2).

width	CPP	Redundacy	Distance	Travel time	Maneuver	Bat Conspt
5	BECD	12.84	4612.5	21.08	125	80
8		18.84	3021.2	13.52	74	52
10		25.52	2339.8	7.4	62	41
12		28.89	2029.9	9.36	62	36
15		12.84	1547.95	7.16	35	28
20		36.59	1126.9	5.25	25	21
5	GBSTC	2.83	4308.4	27.28	365	94
8		3.96	2766.8	16.28	119	62
10		5.73	2089.9	12.07	119	45
12		7.41	1809.7	10.03	85	37
15		8.75	1373.7	7.4	66	29
20		9.36	966.6	5.09	33	20
5	GBWC	9.07	4497.5	28.34	390	94
8		4.26	2789.6	15.01	193	63
10		4.69	2078.4	11.2	98	43
12		14.07	1922.4	9.24	58	35
15		6.25	1360.42	7.02	46	26
20		9.76	1002.8	5.04	25	19

TABLE X. THREE CPP METHODS USING TYPHOON UAV OVER CSUSL PV PLANT (EXPERIMENT 3).

width	CPP	Redundacy	Distance	Travel time	Maneuver	Bat Conspt
1	BECD	8.97	1579.4	9.47	192	35
2		20.05	814.9	5.28	86	20
3		22.09	525.1	3.44	62	14
4		21.11	406.1	3.04	38	11
6		42.86	296.2	2.19	27	9
8		86.67	198.6	1.43	20	7
1	GBSTC	1.25	1289.9	13.1	542	47
2		2.64	680.6	6.23	154	23
3		4.55	448.5	4.15	88	15
4		5.56	370.23	3.23	58	12
6		5.71	233.2	2.08	30	8
8		40	177.3	1.38	19	6
1	GBWC	1.37	1420.7	11.56	462	43
2		4.22	705.9	6.33	168	24
3		11.04	506.1	4.01	69	15
4		8.89	404.4	3.05	44	12
6		13.89	278.7	2.1	24	8
8		13.33	157.5	1.28	14	5

APPENDIX C
TABLES OF IRIS

TABLE XI. 3DR IRIS UAV TECHNICAL SPECIFICATION


3D Robotics Iris	
	
Dimensions	10 cm in height, 55 cm motor-to-motor
Weight	1282 g
Battery	5100 mAh 3S
Camera	N/A
Flight Time	15-20 mins
Flight Speed	11 m/s
Payload Capacity	400 g
Motor	AC 2830, 950 kV

TABLE XII. THREE CPP METHODS USING 3DR IRIS UAV OVER UNIOESTE 1 PV PLANT (EXPERIMENT 4).

width	CPP	Redundacy	Distance	Travel time	Maneuver	Bat Conspt
10	BECD	7.34	3619.1	14.48	45	96
12		13.36	2987.1	12.24	39	80
15		15.33	2391.3	10.04	35	64
17		18.52	2234.1	9.13	25	60
18		13.79	1870.3	7.59	26	52
20		13.33	1773.8	7.25	22	48
10	GBSTC	1.83	3485.5	16.39	100	100
12		2.76	2827	14.12	104	92
15		4.38	2280.3	11.23	74	73
17		6.38	2101.5	10.36	68	68
18		4.6	1790.4	8.52	55	58
20		2.67	1651.2	8.21	54	55
10	GBWC	7.95	3716.5	16.29	83	100
12		11.98	3094.3	14.37	86	95
15		12.41	2442	12.05	78	78
17		14.81	2255.8	10.19	46	67
18		11.49	1883.7	8.47	43	57
20		10.67	1783.3	8.18	39	54

TABLE XIII. THREE CPP METHODS USING 3DR IRIS UAV OVER ARACK PV PLANT (EXPERIMENT 5).

width	CPP	Redundacy	Distance	Travel time	Maneuver	Bat Conspt
7	BECD	15.42	3292.7	15.31	80	95
8		18.84	3020.2	14.2	74	88
10		25.52	2339.3	12.52	62	70
12		28.89	2030.4	9.57	50	60
15		31.25	1548.5	7.27	35	45
20		36.59	1133.3	5.21	25	26
7	GBSTC	5.73	2090.4	43	527	100
8		3.96	2757.8	17.06	179	98
10		5.73	2090.4	12.36	119	76
12		7.41	1809.3	10.18	85	63
15		8.75	13674.2	8	66	48
20		9.76	971	5.07	33	26
5	GBWC	3.66	7270.8	38.41	392	100
8		4.69	2078.8	11.47	98	2
10		4.69	2078.8	11.47	98	71
12		14.07	1922.7	9.43	58	59
15		6.25	1360.08	7.07	46	43
20		6.25	1360.08	7.07	46	25

TABLE XIV. THREE CPP METHODS USING 3DR IRIS UAV OVER CSUSL PV PLANT (EXPERIMENT 6).

width	CPP	Redundacy	Distance	Travel time	Maneuver	Bat Conspt
1	BECD	10.06	1724.8	10.39	211	52
2		15.38	978	6.12	95	30
3		19.3	597.2	4.18	62	21
4		26.67	441.5	3.33	47	17
6		47.22	316.7	2.3	30	12
8		66.67	197.4	1.47	20	9
1	GBSTC	1.77	1416.4	15.31	626	72
2		3.61	697.4	7.2	220	35
3		5.85	508.6	5	108	24
4		5.56	373.4	3.28	65	17
6		19.44	270.1	2.22	32	12
8		40	198.8	1.52	19	9
1	GBWC	3.94	1414.9	15.3	626	72
2		5.53	817.4	7.36	218	38
3		7.6	553	4.36	86	22
4		8.89	404.4	3.05	44	15
6		13.89	274.7	2.13	24	11
8		20	184.9	1.41	16	8

REFERENCES

- [1] C. W. Donovan, *Renewable Energy Finance: Funding the Future of Energy*. World Scientific, 2020.
- [2] D. Gielen, F. Boshell, D. Saygin, M. D. Bazilian, N. Wagner, and R. Gorini, “The role of renewable energy in the global energy transformation,” *Energy Strategy Reviews*, vol. 24, pp. 38–50, 2019.
- [3] H. E. Murdock, D. Gibb, T. André, *et al.*, *Renewables 2020-Global status report*. REN21, 2020.
- [4] S. XM, *Informe anual 2020*. Medellín: XM Compañía de Expertos en Mercados S.A. E.S.P, 2020.
- [5] Y. Castillo, M. C. Gutiérrez, M. Vanegas-Chamorro, G. Valencia, and E. Villicaña, “Rol de las fuentes no convencionales de energía en el sector eléctrico colombiano,” *Prospectiva*, vol. 13, no. 1, pp. 39–51, 2015.
- [6] J. B. Ricardo Ramíres, *Informe de Gestión: 2019*. UPME, 2019.
- [7] C. S. Antonio, B. D. David, C. F. Eduardo, and C. G. M. Alonso, *Generación distribuida, autoconsumo y redes inteligentes*. Editorial UNED, 2015.
- [8] A. Langner, “Photovoltaics Report,” en, p. 50, Jul. 2021.
- [9] S. Gómez Melgar and J. M. Andújar, *Energy efficiency in buildings: Both new and rehabilitated*, 2020.
- [10] A. R. López, A. Krumm, L. Schattenhofer, *et al.*, “Solar pv generation in colombia-a qualitative and quantitative approach to analyze the potential of solar energy market,” *Renewable Energy*, vol. 148, pp. 1266–1279, 2020.
- [11] A. C. Duman and Ö. Güler, “Economic analysis of grid-connected residential rooftop pv systems in turkey,” *Renewable Energy*, vol. 148, pp. 697–711, 2020.
- [12] R. B. Hiremath, B. Kumar, P. Balachandra, N. H. Ravindranath, and B. N. Raghunandan, “Decentralised renewable energy: Scope, relevance and applications in the indian context,” *Energy for Sustainable Development*, vol. 13, no. 1, pp. 4–10, 2009.
- [13] E. Kaplani, “Pv cell and module degradation, detection and diagnostics,” in *Renewable Energy in the Service of Mankind Vol II*, Springer, 2016, pp. 393–402.
- [14] M. Aghaei, A. Dolara, S. Leva, and F. Grimaccia, “Image resolution and defects detection in pv inspection by unmanned technologies,” in *2016 IEEE Power and Energy Society General Meeting (PESGM)*, IEEE, 2016, pp. 1–5.
- [15] M. Koentges, S. Kurtz, C. Packard, *et al.*, *Review of failures of photovoltaic modules*. IEA International Energy Agency, 2014.
- [16] K. Shen, Q. Qiu, Q. Wu, Z. Lin, and Y. Wu, “Research on the development status of photovoltaic panel cleaning equipment based on patent analysis,” in *2019 3rd International Conference on Robotics and Automation Sciences (ICRAS)*, IEEE, 2019, pp. 20–27.
- [17] M. Al-Housani, Y. Bicer, and M. Koç, “Experimental investigations on pv cleaning of large-scale solar power plants in desert climates: Comparison of cleaning techniques for drone retrofitting,” *Energy Conversion and Management*, vol. 185, pp. 800–815, 2019.

- [18] A. K. V. Oliveira, M. Aghaei, U. E. Madukanya, and R. Rüther, "Fault inspection by aerial infrared thermography in a pv plant after a meteorological tsunami," *Revista Brasileira de Energia Solar*, vol. 10, no. 1, pp. 17–25, 2019.
- [19] H. Kawamoto and B. Guo, "Improvement of an electrostatic cleaning system for removal of dust from solar panels," *Journal of Electrostatics*, vol. 91, pp. 28–33, 2018.
- [20] F. P. G. Márquez and I. S. Ramírez, "Condition monitoring system for solar power plants with radiometric and thermographic sensors embedded in unmanned aerial vehicles," *Measurement*, vol. 139, pp. 152–162, 2019.
- [21] E. S. E. Week, *Ridha azaiz*, url<http://https://www.eusew.eu/ridha-azaiz>, 2020. (visited on 10/30/2020).
- [22] S. Gallardo-Saavedra, L. Hernández-Callejo, and O. Duque-Perez, "Image resolution influence in aerial thermographic inspections of photovoltaic plants," *IEEE Transactions on Industrial Informatics*, vol. 14, no. 12, pp. 5678–5686, 2018.
- [23] C. Di Franco and G. Buttazzo, "Coverage path planning for uavs photogrammetry with energy and resolution constraints," *Journal of Intelligent & Robotic Systems*, vol. 83, no. 3, pp. 445–462, 2016.
- [24] Y. Zefri, A. ElKettani, I. Sebari, and S. Ait Lamallam, "Thermal infrared and visual inspection of photovoltaic installations by uav photogrammetry—application case: Morocco," *Drones*, vol. 2, no. 4, p. 41, 2018.
- [25] S. Philipps and W. Warmuth, "Photovoltaics report fraunhofer institute for solar energy systems," in *ISE with support of PSE GmbH November 14th*, FraunhoferISE, 2019.
- [26] W. J. Jamil, H. A. Rahman, S. Shaari, and Z. Salam, "Performance degradation of photovoltaic power system: Review on mitigation methods," *Renewable and Sustainable Energy Reviews*, vol. 67, pp. 876–891, 2017.
- [27] G. Di Lorenzo, R. Araneo, M. Mitolo, A. Niccolai, and F. Grimaccia, "Review of o&m practices in pv plants: Failures, solutions, remote control, and monitoring tools," *IEEE Journal of Photovoltaics*, vol. 10, no. 4, pp. 914–926, 2020.
- [28] G. C. Guerrero-Liquet, S. Oviedo-Casado, J. Sánchez-Lozano, M. S. García-Cascales, J. Prior, and A. Urbina, "Determination of the optimal size of photovoltaic systems by using multi-criteria decision-making methods," *Sustainability*, vol. 10, no. 12, p. 4594, 2018.
- [29] F. Grimaccia, S. Leva, A. Niccolai, and G. Cantoro, "Assessment of pv plant monitoring system by means of unmanned aerial vehicles," in *2018 IEEE International Conference on Environment and Electrical Engineering and 2018 IEEE Industrial and Commercial Power Systems Europe (EEEIC/I&CPS Europe)*, IEEE, 2018, pp. 1–6.
- [30] R. Azaiz, *Flying robot for processing and cleaning smooth, curved and modular surfaces*, US Patent App. 15/118,849, Mar. 2017.
- [31] F. Grimaccia, M. Aghaei, M. Mussetta, S. Leva, and P. B. Quater, "Planning for PV plant performance monitoring by means of unmanned aerial systems (UAS)," *International Journal of Energy and Environmental Engineering*, vol. 6, no. 1, pp. 47–54, Mar. 2015, ISSN: 2251-6832. DOI: 10.1007/s40095-014-0149-6. [Online]. Available: <https://doi.org/10.1007/s40095-014-0149-6>.

- [32] A. M. M. Sizkouhi, M. Aghaei, S. M. Esmailifar, M. R. Mohammadi, and F. Grimaccia, "Automatic boundary extraction of large-scale photovoltaic plants using a fully convolutional network on aerial imagery," *IEEE Journal of Photovoltaics*, vol. 10, no. 4, pp. 1061–1067, 2020.
- [33] S. Leva, M. Aghaei, and F. Grimaccia, "Pv power plant inspection by uas: Correlation between altitude and detection of defects on pv modules," in *2015 IEEE 15th International Conference on Environment and Electrical Engineering (EEEIC)*, IEEE, 2015, pp. 1921–1926.
- [34] F. Grimaccia, S. Leva, A. Dolara, and M. Aghaei, "Survey on pv modules' common faults after an o&m flight extensive campaign over different plants in italy," *IEEE Journal of Photovoltaics*, vol. 7, no. 3, pp. 810–816, 2017.
- [35] P. B. Quater, F. Grimaccia, S. Leva, M. Mussetta, and M. Aghaei, "Light unmanned aerial vehicles (uavs) for cooperative inspection of pv plants," *IEEE Journal of Photovoltaics*, vol. 4, no. 4, pp. 1107–1113, 2014.
- [36] A. K. V. De Oliveira, D. Amstad, U. E. Madukanya, L. R. Do Nascimento, M. Aghaei, and R. R  ther, "Aerial infrared thermography of a cdte utility-scale pv power plant," in *2019 IEEE 46th Photovoltaic Specialists Conference (PVSC)*, IEEE, 2019, pp. 1335–1340.
- [37] M. AGHAEI, "Novel methods in control and monitoring of photovoltaic systems," Publisher: Italy, Ph.D. dissertation, Politecnico di Milano, 2016. [Online]. Available: <https://www.politesi.polimi.it/handle/10589/127023>.
- [38] X. Li, W. Li, Q. Yang, W. Yan, and A. Y. Zomaya, "An Unmanned Inspection System for Multiple Defects Detection in Photovoltaic Plants," *IEEE Journal of Photovoltaics*, vol. 10, no. 2, pp. 568–576, Mar. 2020, Conference Name: IEEE Journal of Photovoltaics, ISSN: 2156-3403. DOI: 10.1109/JPHOTOV.2019.2955183.
- [39] M. Aghaei, A. Gandelli, F. Grimaccia, S. Leva, and R. E. Zich, "Ir real-time analyses for pv system monitoring by digital image processing techniques," in *2015 international conference on event-based control, communication, and signal processing (ebccsp)*, IEEE, 2015, pp. 1–6.
- [40] M. Aghaei, S. Leva, and F. Grimaccia, "Pv power plant inspection by image mosaicing techniques for ir real-time images," in *2016 IEEE 43rd Photovoltaic Specialists Conference (PVSC)*, IEEE, 2016, pp. 3100–3105.
- [41] O. Men  ndez, R. Guam  n, M. P  rez, and F. Auat Cheein, "Photovoltaic modules diagnosis using artificial vision techniques for artifact minimization," *Energies*, vol. 11, no. 7, p. 1688, 2018.
- [42] L. L  pez-Fern  ndez, S. Lag  ela, J. Fern  ndez, and D. Gonz  lez-Aguilera, "Automatic evaluation of photovoltaic power stations from high-density rgb-t 3d point clouds," *Remote Sensing*, vol. 9, no. 6, p. 631, 2017.
- [43] A. Niccolai, F. Grimaccia, and S. Leva, "Advanced asset management tools in photovoltaic plant monitoring: Uav-based digital mapping," *Energies*, vol. 12, no. 24, p. 4736, 2019.
- [44] J. A. Tsanakas, D. Chrysostomou, P. N. Botsaris, and A. Gasteratos, "Fault diagnosis of photovoltaic modules through image processing and canny edge detection on field thermographic measurements," *International Journal of Sustainable Energy*, vol. 34, no. 6, pp. 351–372, 2015.
- [45] Y.-y. Yao and Y.-t. Hu, "Recognition and location of solar panels based on machine vision," in *2017 2nd Asia-Pacific Conference on Intelligent Robot Systems (ACIRS)*, IEEE, 2017, pp. 7–12.

- [46] A. M. M. Sizkouhi, S. M. Esmailifar, M. Aghaei, A. K. V. De Oliveira, and R. R  ther, "Autonomous path planning by unmanned aerial vehicle (uav) for precise monitoring of large-scale pv plants," in *2019 IEEE 46th Photovoltaic Specialists Conference (PVSC)*, IEEE, 2019, pp. 1398–1402.
- [47] E. Rodriguez-Esparza, L. A. Zanella-Calzada, D. Oliva, *et al.*, "An efficient harris hawks-inspired image segmentation method," *Expert Systems with Applications*, vol. 155, p. 113 428, 2020.
- [48] A. Garcia-Garcia, S. Orts-Escolano, S. Oprea, V. Villena-Martinez, P. Martinez-Gonzalez, and J. Garcia-Rodriguez, "A survey on deep learning techniques for image and video semantic segmentation," *Applied Soft Computing*, vol. 70, pp. 41–65, 2018.
- [49] N. R. Pal and S. K. Pal, "A review on image segmentation techniques," *Pattern recognition*, vol. 26, no. 9, pp. 1277–1294, 1993.
- [50] T. Hoeser and C. Kuenzer, "Object detection and image segmentation with deep learning on earth observation data: A review-part i: Evolution and recent trends," *Remote Sensing*, vol. 12, no. 10, p. 1667, 2020.
- [51] C. Henry, S. Poudel, S.-W. Lee, and H. Jeong, "Automatic detection system of deteriorated pv modules using drone with thermal camera," *Applied Sciences*, vol. 10, no. 11, p. 3802, 2020.
- [52] J. Long, E. Shelhamer, and T. Darrell, "Fully convolutional networks for semantic segmentation," in *Proceedings of the IEEE conference on computer vision and pattern recognition*, 2015, pp. 3431–3440.
- [53] S. Puttemans, W. Van Ranst, and T. Goedem  , "Detection of photovoltaic installations in rgb aerial imaging: A comparative study," *GEOBIA 2016 proceedings*, 2016.
- [54] M. S. Karoui, F. Z. Benhalouche, and Deville, "Partial linear nmf-based unmixing methods for detection and area estimation of photovoltaic panels in urban hyperspectral remote sensing data," *Remote Sensing*, vol. 11, pp. 2164–2170, 2019.
- [55] S. Bhatnagar, L. Gill, and B. Ghosh, "Drone image segmentation using machine and deep learning for mapping raised bog vegetation communities," *Remote Sensing*, vol. 12, no. 16, 2020, ISSN: 2072-4292. DOI: 10.3390/rs12162602. [Online]. Available: <https://www.mdpi.com/2072-4292/12/16/2602>.
- [56] C. Sothe, C. M. D. Almeida, M. B. Schimalski, *et al.*, "A comparison of machine and deep-learning algorithms applied to multisource data for a subtropical forest area classification," *International Journal of Remote Sensing*, vol. 41, no. 5, pp. 1943–1969, 2020. DOI: 10.1080/01431161.2019.1681600. eprint: <https://doi.org/10.1080/01431161.2019.1681600>. [Online]. Available: <https://doi.org/10.1080/01431161.2019.1681600>.
- [57] O. Ronneberger, P. Fischer, and T. Brox, "U-net: Convolutional networks for biomedical image segmentation," in *International Conference on Medical image computing and computer-assisted intervention*, Springer, 2015, pp. 234–241.
- [58] M. Ren and R. S. Zemel, "End-to-end instance segmentation with recurrent attention," in *Proceedings of the IEEE conference on computer vision and pattern recognition*, 2017, pp. 6656–6664.

- [59] B. T. McCollum, "Analyzing gps accuracy through the implementation of low-cost cots real-time kinematic gps receivers in unmanned aerial systems," AIR FORCE INSTITUTE OF TECHNOLOGY WRIGHT-PATTERSON AFB OH WRIGHT-PATTERSON . . . , Tech. Rep., 2017.
- [60] ardupilot.org, *Mission Planner Home — Mission Planner documentation*. [Online]. Available: <https://ardupilot.org/planner/> (visited on 07/07/2021).
- [61] G. Donald, *QGroundControl Ground Control Station*, original-date: 2011-10-13T07:31:07Z, Aug. 2021. [Online]. Available: <https://github.com/mavlink/qgroundcontrol> (visited on 09/23/2021).
- [62] M. Sizkouhi, M. Aghaei, and S. M. Esmailifar, *Aerial imagery of pv plants for boundary detection*, 2020. DOI: 10.21227/g2bb-ms79. [Online]. Available: <https://dx.doi.org/10.21227/g2bb-ms79>.
- [63] J. Canny, "A computational approach to edge detection," *IEEE Transactions on Pattern Analysis and Machine Intelligence*, vol. PAMI-8, no. 6, pp. 679–698, 1986. DOI: 10.1109/TPAMI.1986.4767851.
- [64] M. R. Berthold, C. Borgelt, F. Höppner, F. Klawonn, and R. Silipo, "Data preparation," in *Guide to Intelligent Data Science*, Springer, 2020, pp. 127–156.
- [65] A. Abdollahi, B. Pradhan, and A. M. Alamri, "An ensemble architecture of deep convolutional segnet and unet networks for building semantic segmentation from high-resolution aerial images," *Geocarto International*, pp. 1–16, 2020.
- [66] S. Minaee, Y. Y. Boykov, F. Porikli, A. J. Plaza, N. Kehtarnavaz, and D. Terzopoulos, "Image segmentation using deep learning: A survey," *IEEE Transactions on Pattern Analysis and Machine Intelligence*, 2021.
- [67] S. Hao, Y. Zhou, and Y. Guo, "A brief survey on semantic segmentation with deep learning," *Neurocomputing*, vol. 406, pp. 302–321, 2020.
- [68] F. Lateef and Y. Ruichek, "Survey on semantic segmentation using deep learning techniques," *Neurocomputing*, vol. 338, pp. 321–348, 2019.
- [69] K. Simonyan and A. Zisserman, "Very deep convolutional networks for large-scale image recognition," *arXiv preprint arXiv:1409.1556*, 2014.
- [70] M. Cao, Y. Zou, D. Yang, and C. Liu, "Gisca: Gradient-inductive segmentation network with contextual attention for scene text detection," *IEEE Access*, vol. 7, pp. 62 805–62 816, 2019.
- [71] N. Shibuya, "Up-sampling with transposed convolution," *Towards Data Science*, 2017.
- [72] Martín Abadi, Ashish Agarwal, Paul Barham, *et al.*, *TensorFlow: Large-scale machine learning on heterogeneous systems*, Software available from tensorflow.org, 2015. [Online]. Available: <https://www.tensorflow.org/>.
- [73] G. Alain and Y. Bengio, "What regularized auto-encoders learn from the data-generating distribution," *The Journal of Machine Learning Research*, vol. 15, no. 1, pp. 3563–3593, 2014.
- [74] D. Yi, J. Ahn, and S. Ji, "An effective optimization method for machine learning based on adam," *Applied Sciences*, vol. 10, no. 3, p. 1073, 2020.
- [75] M. Rizzi and C. Guaragnella, "Skin lesion segmentation using image bit-plane multilayer approach," *Applied Sciences*, vol. 10, no. 9, p. 3045, 2020.

- [76] M. Talal, A. Panthakkan, H. Mukhtar, W. Mansoor, S. Almansoori, and H. Al Ahmad, "Detection of water-bodies using semantic segmentation," in *2018 International Conference on Signal Processing and Information Security (ICSPIS)*, IEEE, 2018, pp. 1–4.
- [77] D. M. Powers, "Evaluation: From precision, recall and f-measure to roc, informedness, markedness and correlation," *arXiv preprint arXiv:2010.16061*, 2020.
- [78] N. Alalwan, A. Abozeid, A. A. ElHabshy, and A. Alzahrani, "Efficient 3d deep learning model for medical image semantic segmentation," *Alexandria Engineering Journal*, vol. 60, no. 1, pp. 1231–1239, 2021.
- [79] J. Yu, Z. Wang, A. Majumdar, and R. Rajagopal, "Deepsolar: A machine learning framework to efficiently construct a solar deployment database in the united states," *Joule*, vol. 2, no. 12, pp. 2605–2617, 2018.
- [80] C. Elkin, "Sun roof project," Google, [online]:Available <http://google.com/get/sunroof>. 2015.
- [81] NREL, "Open pv project," U.S. Department of Energy's Solar Energy Technologies Office, [online]:Available <https://www.energy.gov/eere/solarpoweringamerica/open-pv-project>, 2018.
- [82] M. G. F. Costa, J. P. M. Campos, G. d. A. e Aquino, W. C. de Albuquerque Pereira, and C. F. F. Costa Filho, "Evaluating the performance of convolutional neural networks with direct acyclic graph architectures in automatic segmentation of breast lesion in us images," *BMC medical imaging*, vol. 19, no. 1, pp. 1–13, 2019.
- [83] A. Perez, *Andresperez86/BoundaryExtractionPhotovoltaicPlants*, original-date: 2021-05-25T22:10:45Z, Apr. 2021. [Online]. Available: <https://github.com/andresperez86/BoundaryExtractionPhotovoltaicPlants> (visited on 05/25/2021).
- [84] L. Qiongyan, J. Cai, B. Berger, M. Okamoto, and S. J. Miklavcic, "Detecting spikes of wheat plants using neural networks with laws texture energy," *Plant Methods*, vol. 13, no. 1, pp. 1–13, 2017.
- [85] Z. Ling, D. Zhang, R. C. Qiu, *et al.*, "An accurate and real-time method of self-blast glass insulator location based on faster r-cnn and u-net with aerial images," *CSEE Journal of Power and Energy Systems*, vol. 5, no. 4, pp. 474–482, 2019.
- [86] REN21[®], *Global status reports*, English, (accessed on 14 August 2021), Jun. 2021. [Online]. Available: <https://www.ren21.net/reports/global-status-report/>.
- [87] M. Alkhraijah, M. Alowaifeer, M. Alsaleh, A. Alfaris, and D. K. Molzahn, "The effects of social distancing on electricity demand considering temperature dependency," *Energies*, vol. 14, no. 2, 2021, ISSN: 1996-1073. DOI: 10.3390/en14020473. [Online]. Available: <https://www.mdpi.com/1996-1073/14/2/473>.
- [88] A. Mey, *Most U.S. utility-scale solar photovoltaic power plants are 5 megawatts or smaller - Today in Energy - U.S. Energy Information Administration (EIA)*. [Online]. Available: <https://www.eia.gov/todayinenergy/detail.php?id=38272#> (visited on 10/03/2021).
- [89] H. M. Maghrabie, M. A. Abdelkareem, A. H. Al-Alami, *et al.*, "State-of-the-art technologies for building-integrated photovoltaic systems," *Buildings*, vol. 11, 2021, ISSN: 2075-5309. DOI: 10.3390/buildings11090383. [Online]. Available: <https://www.mdpi.com/2075-5309/11/9/383>.

- [90] P. Hao, Y. Zhang, H. Lu, and Z. Lang, "A novel method for parameter identification and performance estimation of PV module under varying operating conditions," *Energy Conversion and Management*, vol. 247, p. 114689, 2021, ISSN: 0196-8904. DOI: <https://doi.org/10.1016/j.enconman.2021.114689>. [Online]. Available: <https://www.sciencedirect.com/science/article/pii/S0196890421008657>.
- [91] IRENA, *Future of solar photovoltaic: Deployment, investment, technology, grid integration, and socio-economic aspects*, (accessed on 24 oct 2021), 2019. [Online]. Available: [Available%20online:%20%7Bhttps://www.irena.org%7D](https://www.irena.org).
- [92] V. Poulek, J. Šafránková, L. Černá, *et al.*, "Pv panel and pv inverter damages caused by combination of edge delamination, water penetration, and high string voltage in moderate climate," *IEEE Journal of Photovoltaics*, vol. 11, no. 2, pp. 561–565, 2021. DOI: 10.1109/JPHOTOV.2021.3050984.
- [93] L. Narvarte, J. Fernández-Ramos, F. Martínez-Moreno, L. Carrasco, R. Almeida, and I. Carrêlo, "Solutions for adapting photovoltaics to large power irrigation systems for agriculture," *Sustainable Energy Technologies and Assessments*, vol. 29, pp. 119–130, 2018, ISSN: 2213-1388. DOI: <https://doi.org/10.1016/j.seta.2018.07.004>. [Online]. Available: <https://www.sciencedirect.com/science/article/pii/S2213138818301759>.
- [94] M. Libra, M. Daneček, J. Lešetický, V. Poulek, J. Sedláček, and V. Beránek, "Monitoring of defects of a photovoltaic power plant using a drone," *Energies*, vol. 12, no. 5, p. 795, 2019.
- [95] X. Li, W. Li, Q. Yang, W. Yan, and A. Y. Zomaya, "An unmanned inspection system for multiple defects detection in photovoltaic plants," *IEEE Journal of Photovoltaics*, vol. 10, no. 2, pp. 568–576, 2019.
- [96] M. Alsafasfeh, I. Abdel-Qader, B. Bazuin, Q. Alsafasfeh, and W. Su, "Unsupervised fault detection and analysis for large photovoltaic systems using drones and machine vision," *Energies*, vol. 11, no. 9, p. 2252, 2018.
- [97] S. Gallardo-Saavedra, E. Franco-Mejia, L. Hernández-Callejo, Ó. Duque-Pérez, H. Loaiza-Correa, and E. Alfaro-Mejia, "Aerial thermographic inspection of photovoltaic plants: Analysis and selection of the equipment," in *2017 Proceedings ISES Solar World Congress, IEA SHC*, 2017.
- [98] A. Niccolai, F. Grimaccia, and S. Leva, "Advanced asset management tools in photovoltaic plant monitoring: Uav-based digital mapping," *Energies*, vol. 12, no. 24, 2019, ISSN: 1996-1073. DOI: 10.3390/en12244736. [Online]. Available: <https://www.mdpi.com/1996-1073/12/24/4736>.
- [99] N. J. Thrower and J. R. Jensen, "The orthophoto and orthophotomap: Characteristics, development and application," *The American Cartographer*, vol. 3, no. 1, pp. 39–56, 1976.
- [100] S. Leva and M. Aghaei, "Power engineering: Advances and challenges part b: Electrical power," in *Chapter 3: Failures and Defects in PV systems review and Methods of Analysis*, Taylor & Francis Group, CRC press, 2018.
- [101] D. Kim, J. Youn, and C. Kim, "Automatic photovoltaic panel area extraction from uav thermal infrared images," *Journal of the Korean Surveying Society*, vol. 34, no. 6, pp. 559–568, 2016.

- [102] X. Li, Q. Yang, Z. Lou, and W. Yan, "Deep learning based module defect analysis for large-scale photovoltaic farms," *IEEE Transactions on Energy Conversion*, vol. 34, no. 1, pp. 520–529, 2019. DOI: 10.1109/TEC.2018.2873358.
- [103] Y. Ding, R. Cao, S. Liang, F. Qi, Q. Yang, and W. Yan, "Density-based optimal uav path planning for photovoltaic farm inspection in complex topography," in *2020 Chinese Control And Decision Conference (CCDC)*, IEEE, 2020, pp. 3931–3936.
- [104] X. Luo, X. Li, Q. Yang, *et al.*, "Optimal path planning for uav based inspection system of large-scale photovoltaic farm," in *2017 Chinese Automation Congress (CAC)*, 2017, pp. 4495–4500. DOI: 10.1109/CAC.2017.8243572.
- [105] E. Salahat, C.-A. Asselineau, J. Coventry, and R. Mahony, "Waypoint planning for autonomous aerial inspection of large-scale solar farms," in *IECON 2019 - 45th Annual Conference of the IEEE Industrial Electronics Society*, vol. 1, 2019, pp. 763–769. DOI: 10.1109/IECON.2019.8927123.
- [106] H. M. Choset, K. M. Lynch, S. Hutchinson, *et al.*, *Principles of robot motion: theory, algorithms, and implementation*. MIT press, 2005.
- [107] T. M. Cabreira, L. B. Brisolará, and P. R. Ferreira Jr, "Survey on coverage path planning with unmanned aerial vehicles," *Drones*, vol. 3, no. 1, p. 4, 2019.
- [108] Y. B. Sebbane, *Intelligent autonomy of UAVs: advanced missions and future use*. CRC Press, 2018.
- [109] H. Choset, "Coverage for robotics—a survey of recent results," *Annals of mathematics and artificial intelligence*, vol. 31, no. 1, pp. 113–126, 2001.
- [110] P. Veerajagadheswar, K. Ping-Cheng, M. R. Elara, A. V. Le, and M. Iwase, "Motion planner for a tetris-inspired reconfigurable floor cleaning robot," *International Journal of Advanced Robotic Systems*, vol. 17, no. 2, p. 1 729 881 420 914 441, 2020.
- [111] M. Coombes, T. Fletcher, W.-H. Chen, and C. Liu, "Optimal polygon decomposition for uav survey coverage path planning in wind," *Sensors*, vol. 18, no. 7, 2018, ISSN: 1424-8220. DOI: 10.3390/s18072132. [Online]. Available: <https://www.mdpi.com/1424-8220/18/7/2132>.
- [112] N. Islam, M. M. Rashid, F. Pasandideh, B. Ray, S. Moore, and R. Kadel, "A review of applications and communication technologies for internet of things (iot) and unmanned aerial vehicle (uav) based sustainable smart farming," *Sustainability*, vol. 13, no. 4, p. 1821, 2021.
- [113] H. X. Pham, H. M. La, D. Feil-Seifer, and M. Deans, "A distributed control framework for a team of unmanned aerial vehicles for dynamic wildfire tracking," in *2017 IEEE/RSJ International Conference on Intelligent Robots and Systems (IROS)*, IEEE, 2017, pp. 6648–6653.
- [114] D. Kaljaca, B. Vroegindewei, and E. van Henten, "Coverage trajectory planning for a bush trimming robot arm," *Journal of Field Robotics*, vol. 37, no. 2, pp. 283–308, 2020.
- [115] W. Chang, G. Yang, J. Yu, Z. Liang, L. Cheng, and C. Zhou, "Development of a power line inspection robot with hybrid operation modes," in *2017 IEEE/RSJ International Conference on Intelligent Robots and Systems (IROS)*, IEEE, 2017, pp. 973–978.
- [116] S. S. Mansouri, C. Kanellakis, E. Fresk, D. Kominiak, and G. Nikolakopoulos, "Cooperative coverage path planning for visual inspection," *Control Engineering Practice*, vol. 74, pp. 118–131, 2018, ISSN: 0967-0661. DOI: <https://doi.org/10.1016/j.conengprac.2018.03.002>. [Online]. Available: <https://www.sciencedirect.com/science/article/pii/S0967066118300315>.

- [117] E. Galceran and M. Carreras, "A survey on coverage path planning for robotics," *Robotics and Autonomous systems*, vol. 61, no. 12, pp. 1258–1276, 2013.
- [118] R. Bormann, F. Jordan, J. Hampp, and M. Hägele, "Indoor coverage path planning: Survey, implementation, analysis," in *2018 IEEE International Conference on Robotics and Automation (ICRA)*, IEEE, 2018, pp. 1718–1725.
- [119] L. Nam, L. Huang, X. Li, and J. Xu, "An approach for coverage path planning for UAVs," in *2016 IEEE 14th International Workshop on Advanced Motion Control, AMC 2016*, 2016, pp. 411–416, ISBN: 9781479984640. DOI: 10.1109/AMC.2016.7496385.
- [120] R. Dai, S. Fotedar, M. Radmanesh, and M. Kumar, "Quality-aware uav coverage and path planning in geometrically complex environments," *Ad Hoc Networks*, vol. 73, pp. 95–105, 2018.
- [121] P. Yao, Y. Cai, and Q. Zhu, "Time-optimal trajectory generation for aerial coverage of urban building," *Aerospace Science and Technology*, vol. 84, pp. 387–398, 2019.
- [122] A. Majeed and S. Lee, "A new coverage flight path planning algorithm based on footprint sweep fitting for unmanned aerial vehicle navigation in urban environments," *Applied Sciences*, vol. 9, no. 7, p. 1470, 2019.
- [123] A. Elfes, M. Campos, M. Bergerman, S. Bueno, and G. Podnar, "A robotic unmanned aerial vehicle for environmental research and monitoring," in *Proceedings of the First Scientific Conference on the Large Scale Biosphere-Atmosphere Experiment in Amazonia (LBA)*, 2000, pp. 12 630–000.
- [124] A. Saeed, A. Abdelkader, M. Khan, A. Neishaboori, K. A. Harras, and A. Mohamed, "On realistic target coverage by autonomous drones," *ACM Transactions on Sensor Networks (TOSN)*, vol. 15, no. 3, pp. 1–33, 2019.
- [125] F. Lingelbach, "Path planning using probabilistic cell decomposition," in *IEEE International Conference on Robotics and Automation, 2004. Proceedings. ICRA'04. 2004*, IEEE, vol. 1, 2004, pp. 467–472.
- [126] Z. Khanam, S. Saha, S. Ehsan, R. Stolkin, and K. Mcdonald-Maier, "Coverage path planning techniques for inspection of disjoint regions with precedence provision," *IEEE Access*, vol. 9, pp. 5412–5427, 2021. DOI: 10.1109/ACCESS.2020.3044987.
- [127] W. Khiati, Y. Moumen, A. E. Habchi, I. Zerrouk, J. Berrich, and T. Bouchentouf, "Grid based approach (gba): A new approach based on the grid-clustering algorithm to solve a cpp type problem for air surveillance using uavs," in *2020 Fourth International Conference On Intelligent Computing in Data Sciences (ICDS)*, 2020, pp. 1–5. DOI: 10.1109/ICDS50568.2020.9268683.
- [128] M. Juliá, A. Gil, and O. Reinoso, "A comparison of path planning strategies for autonomous exploration and mapping of unknown environments," *Autonomous Robots*, vol. 33, no. 4, pp. 427–444, Nov. 2012, ISSN: 1573-7527. DOI: 10.1007/s10514-012-9298-8. [Online]. Available: <https://doi.org/10.1007/s10514-012-9298-8>.
- [129] A. Pérez-González, Á. Jaramillo-Duque, and J. B. Cano-Quintero, "Automatic boundary extraction for photovoltaic plants using the deep learning unet model," *Applied Sciences*, vol. 11, no. 14, 2021, ISSN: 20763417. DOI: 10.3390/app11146524. [Online]. Available: <https://www.mdpi.com/2076-3417/11/14/6524>.

- [130] C. Coopmans, M. Podhradský, and N. V. Hoffer, “Software-and hardware-in-the-loop verification of flight dynamics model and flight control simulation of a fixed-wing unmanned aerial vehicle,” in *2015 Workshop on Research, Education and Development of Unmanned Aerial Systems (RED-UAS)*, IEEE, 2015, pp. 115–122.
- [131] G. Roggi, A. Niccolai, F. Grimaccia, and M. Lovera, “A computer vision line-tracking algorithm for automatic uav photovoltaic plants monitoring applications,” *Energies*, vol. 13, no. 4, 2020, ISSN: 1996-1073. DOI: 10.3390/en13040838. [Online]. Available: <https://www.mdpi.com/1996-1073/13/4/838>.
- [132] E. M. Coates and T. I. Fossen, “Geometric reduced-attitude control of fixed-wing uavs,” *Applied Sciences*, vol. 11, no. 7, 2021, ISSN: 2076-3417. DOI: 10.3390/app11073147. [Online]. Available: <https://www.mdpi.com/2076-3417/11/7/3147>.
- [133] A. Tullu, B. Endale, A. Wondosen, and H.-Y. Hwang, “Machine learning approach to real-time 3d path planning for autonomous navigation of unmanned aerial vehicle,” *Applied Sciences*, vol. 11, no. 10, 2021, ISSN: 2076-3417. DOI: 10.3390/app11104706. [Online]. Available: <https://www.mdpi.com/2076-3417/11/10/4706>.
- [134] L. Pitonakova, M. Giuliani, A. Pipe, and A. Winfield, “Feature and performance comparison of the v-rep, gazebo and argos robot simulators,” in *Annual Conference Towards Autonomous Robotic Systems*, Springer, 2018, pp. 357–368.
- [135] M. Akcakoca, B. M. Atici, B. Gever, *et al.*, “A simulation-based development and verification architecture for micro uav teams and swarms,” in *AIAA Scitech 2019 Forum*, 2019, p. 1979.
- [136] *Unoeste terá maior usina solar de geração distribuída de SP - Unoeste*, pt-br. [Online]. Available: [Available%20online:%7Bhttp://www.unoeste.br/noticias/2019/3/unoeste-tera-maior-usina-solar-de-geracao-distribuida-de-sp%7D](http://www.unoeste.br/noticias/2019/3/unoeste-tera-maior-usina-solar-de-geracao-distribuida-de-sp) (visited on 10/11/2021).
- [137] *ABA Newsletter*. [Online]. Available: [Available%20online:%20%7Bhttp://www.csus.edu/aba2/newsletters/fall2012/abagreennews.html%7D](http://www.csus.edu/aba2/newsletters/fall2012/abagreennews.html) (visited on 10/11/2021).
- [138] M. Abadi, P. Barham, J. Chen, *et al.*, “Tensorflow: A system for large-scale machine learning,” in *12th USENIX Symposium on Operating Systems Design and Implementation (OSDI 16)*, Savannah, GA: USENIX Association, Nov. 2016, pp. 265–283, ISBN: 978-1-931971-33-1. [Online]. Available: <https://www.usenix.org/conference/osdi16/technical-sessions/presentation/abadi>.
- [139] *Flask*, original-date: 2010-04-06T11:11:59Z, Oct. 2021. [Online]. Available: [Available%20online:%20%7Bhttps://flask.palletsprojects.com/en/2.0.x/%7D](https://flask.palletsprojects.com/en/2.0.x/) (visited on 10/31/2021).
- [140] *Mavlink*, original-date: 2011-08-12T06:51:52Z, Oct. 2021. [Online]. Available: <https://github.com/mavlink/mavlink> (visited on 10/24/2021).
- [141] J. Li, Y. Zhou, and L. Lamont, “Communication architectures and protocols for networking unmanned aerial vehicles,” in *2013 IEEE Globecom Workshops (GC Wkshps)*, 2013, pp. 1415–1420. DOI: 10.1109/GLOCOMW.2013.6825193.
- [142] I. H. Sarker, “Machine Learning: Algorithms, Real-World Applications and Research Directions,” *SN Computer Science*, vol. 2, no. 3, p. 160, Mar. 2021, ISSN: 2661-8907. DOI: 10.1007/s42979-021-00592-x. [Online]. Available: <https://doi.org/10.1007/s42979-021-00592-x>.

- [143] G. Bradski, “The opencv library.,” *Dr. Dobb’s Journal: Software Tools for the Professional Programmer*, vol. 25, no. 11, pp. 120–123, 2000.
- [144] *OpenCV: OpenCV-Python Tutorials*. [Online]. Available: https://docs.opencv.org/master/d6/d00/tutorial_py_root.html (visited on 10/18/2021).
- [145] H. Choset and P. Pignon, “Coverage path planning: The boustrophedon cellular decomposition,” in *Field and service robotics*, Springer, 1998, pp. 203–209.
- [146] Y. Gabriely and E. Rimon, “Spanning-tree based coverage of continuous areas by a mobile robot,” *Annals of Mathematics and Artificial Intelligence*, vol. 31, no. 1, pp. 77–98, Oct. 2001, ISSN: 1573-7470. DOI: 10.1023/A:1016610507833. [Online]. Available: <https://doi.org/10.1023/A:1016610507833>.
- [147] A. Zelinsky, R. A. Jarvis, J. Byrne, S. Yuta, *et al.*, “Planning paths of complete coverage of an unstructured environment by a mobile robot,” in *Proceedings of international conference on advanced robotics*, Citeseer, vol. 13, 1993, pp. 533–538.
- [148] N. M. Ceballos, J. Valencia, and A. A. Giraldo, “Simulation and assessment educational framework for mobile robot algorithms,” *Journal of Automation, Mobile Robotics and Intelligent Systems*, pp. 53–59, 2014.
- [149] L. Jaeyoung, *PX4 Gazebo Plugin Suite for MAVLink SITL and HITL*, original-date: 2016-01-02T19:02:58Z, Dec. 2021. [Online]. Available: https://github.com/PX4/PX4-SITL_gazebo/blob/ffb87ef4a312564cf91791bd5a9d683aacd085a6/models/iris/iris.sdf.jinja (visited on 12/07/2021).
- [150] M. Paradzik and G. İnce, “Multi-agent search strategy based on digital pheromones for uavs,” in *2016 24th Signal Processing and Communication Application Conference (SIU)*, 2016, pp. 233–236. DOI: 10.1109/SIU.2016.7495720.
- [151] M. Torres, D. A. Pelta, J. L. Verdegay, and J. C. Torres, “Coverage path planning with unmanned aerial vehicles for 3d terrain reconstruction,” *Expert Systems with Applications*, vol. 55, pp. 441–451, 2016.
- [152] J. Araújo, P. Sujit, and J. Sousa, “Multiple uav area decomposition and coverage,” in *2013 IEEE Symposium on Computational Intelligence for Security and Defense Applications (CISDA)*, 2013, pp. 30–37. DOI: 10.1109/CISDA.2013.6595424.
- [153] *PX4 Drone Autopilot*, original-date: 2012-08-04T21:19:36Z, 2021. [Online]. Available: <https://github.com/PX4/PX4-Autopilot> (visited on 09/23/2021).
- [154] N. Koenig and A. Howard, “Design and use paradigms for gazebo, an open-source multi-robot simulator,” in *2004 IEEE/RSJ International Conference on Intelligent Robots and Systems (IROS) (IEEE Cat. No.04CH37566)*, vol. 3, 2004, 2149–2154 vol.3. DOI: 10.1109/IROS.2004.1389727.
- [155] M. Quigley, K. Conley, B. Gerkey, *et al.*, “Ros: An open-source robot operating system,” in *ICRA workshop on open source software*, Kobe, Japan, 2009, p. 5.
- [156] G. Silano and L. Iannelli, “CrazyS: A Software-in-the-Loop Simulation Platform for the Crazyflie 2.0 Nano-Quadcopter,” in *Robot Operating System (ROS): The Complete Reference (Volume 4)*, A. Koubaa, Ed., Cham: Springer International Publishing, 2020, pp. 81–115, ISBN: 978-3-030-20190-6. DOI: 10.1007/978-3-030-20190-6_4. [Online]. Available: https://doi.org/10.1007/978-3-030-20190-6_4.

- [157] F. E. Salamh, U. Karabiyik, and M. K. Rogers, “Rpas forensic validation analysis towards a technical investigation process: A case study of yuneec typhoon h,” *Sensors*, vol. 19, no. 15, 2019, ISSN: 1424-8220. DOI: 10.3390/s19153246. [Online]. Available: <https://www.mdpi.com/1424-8220/19/15/3246>.
- [158] *Yuneec Typhoon H - Yuneec Futurhobby*, es. [Online]. Available: <https://yuneec-futurhobby.com/yuneec-typhoon-h-pro-realsense> (visited on 10/28/2021).
- [159] *3DR Iris - the ready to fly UAV Quadcopter*. [Online]. Available: <http://www.arducopter.co.uk/iris-quadcopter-uav.html> (visited on 10/28/2021).
- [160] S. H. Tan and J. Md Ali, “Quartic and quintic polynomial interpolation,” in *AIP Conference Proceedings*, American Institute of Physics, 2013, pp. 664–675.
- [161] A. Pérez-González, *Andresperez86/Cpp_gui*, Available online: https://github.com/andresperez86/Cpp_GUI (accessed on 29 oct 2021), original-date: 2021-08-13T00:08:22Z, Aug. 2021. (visited on 10/28/2021).
- [162] S. Jordan, J. Moore, S. Hovet, *et al.*, “State-of-the-art technologies for UAV inspections,” *IET Radar, Sonar and Navigation*, vol. 12, no. 2, pp. 151–164, 2018, ISSN: 17518784. DOI: 10.1049/iet-rsn.2017.0251.
- [163] A. Ghaddar, A. Merei, and E. Natalizio, “Pps: Energy-aware grid-based coverage path planning for uavs using area partitioning in the presence of nfzs,” *Sensors*, vol. 20, no. 13, 2020, ISSN: 1424-8220. DOI: 10.3390/s20133742. [Online]. Available: <https://www.mdpi.com/1424-8220/20/13/3742>.
- [164] G. Öst, *Search path generation with uav applications using approximate convex decomposition*, 2012.